Catalyst warm-up to light-off by pulsating engine exhaust: two-dimensional studies

Benjamin, S.F. and Roberts, C.A.

Author post-print (accepted) deposited in CURVE June 2013

Original citation & hyperlink:
Benjamin, S.F. and Roberts, C.A. (2004) Catalyst warm-up to light-off by pulsating engine exhaust: two-dimensional studies. International Journal of Engine Research, volume 5 (3): 257-280.
http://dx.doi.org/10.1243/1468087041549607

Copyright © and Moral Rights are retained by the author(s) and/ or other copyright owners. A copy can be downloaded for personal non-commercial research or study, without prior permission or charge. This item cannot be reproduced or quoted extensively from without first obtaining permission in writing from the copyright holder(s). The content must not be changed in any way or sold commercially in any format or medium without the formal permission of the copyright holders.

This document is the author's post-print version of the journal article, incorporating any revisions agreed during the peer-review process. Some differences between the published version and this version may remain and you are advised to consult the published version if you wish to cite from it.

CURVE is the Institutional Repository for Coventry University
http://curve.coventry.ac.uk/open

CATALYST WARM-UP TO LIGHT-OFF BY PULSATING ENGINE EXHAUST: 2D STUDIES

S. F. Benjamin and C. A. Roberts

School of Engineering, Coventry University, CV1 5FB, UK

Email: s.benjamin@coventry.ac.uk

ABSTRACT

This paper presents the results of two-dimensional (2D) studies on a range of different catalyst substrates warmed by exhaust from a four-cylinder gasoline engine. Engine speeds investigated were 2000 and 3000 rpm, corresponding to frequencies of 67 and 100 Hz. Of the nine substrates investigated, four were washcoated but non-reactive, and four were washcoated and reactive. The ninth substrate was a hybrid sample with its front end inactive and its downstream end active: this is analogous to an aged catalyst. The temperature at sixteen locations within the substrates was measured. All the substrates were warmed by the pulsating exhaust flow from an engine running lean of stoichiometric. The reactive substrates were warmed through light-off and both substrate temperatures and hydrocarbon conversion were monitored. The latter was measured with very high response time fast flame ionisation detectors. Predicted temperatures and conversion were obtained from a 2D CFD model. The model was based on the porous medium approach and incorporated a simple chemical scheme for oxidation under lean conditions. Standard values for reaction rate constants were found to be accurate for the lean conditions studied. Comparison was made of measurements of temperature and conversion fraction with predictions, with particular reference to the time taken to achieve light-off. Steady flow CFD predictions were found to be in good overall agreement with engine test data. Pulsing flow CFD predictions were found, however, to improve on the degree of agreement for warm-up of non-reactive samples, but at the expense of increased computation time. The performance of the reactive hybrid sample was accurately predicted by adjustment of the parameter for active area per unit volume, providing the basis for a technique for prediction of performance for aged catalysts.

KEY WORDS

automotive catalyst, light-off, pulsating flow, engine test, substrate temperature, hydrocarbon conversion

NOTATION

A_c surface area of Pt per unit volume of catalyst monolith, m^2/m^3

A_v wetted surface area per unit volume of catalyst monolith, m^2/m^3

c_w thermal capacity of substrate wall material, J /(kg K)

c_{pg} thermal capacity of gas or air, J /(kg K)

C_{si} concentration of species i at reactive surface

C_{gi} concentration of species i in gas stream

d diameter of monolithic substrate, m

D depth at which thermocouple is located in substrate, d/2 – r, m

d_h hydraulic diameter of substrate channel, m

E_i activation energy for species i, J /mol

G denominator defined by equation (10)

h heat transfer coefficient, W /(m^2 K)

ΔH_i heat of reaction of species i, J /mol

k thermal conductivity of air, W /(m K)

k_1 , k_2 pre-exponential frequency factors, mol K /(s m^2 Pt)

k_{ax} axial thermal conductivity of bulk substrate, W /(m K)

k_{rad} radial thermal conductivity of bulk substrate, W /(m K)

K_{mi} mass transfer coefficient, m /s

m' mass flow rate per unit substrate face area, mass flux, kg / (s m^2)

M mass flow rate, kg /s

M_i molar mass of species i, kg /mol

Nu Nusselt number, h d_h / k

r radial co-ordinate, m

R gas constant, J /(mol K)

Re Reynolds number based on inlet pipe diameter

R_i reaction rate for species i, mol /(s m^3)

S source term in species transport equation, kg /(s m^3)

S_e additional source term in enthalpy equation due to heats of reaction, J /(s m^3)

t time, s

t_r residence time in computational cell, s

Δt time step for computations, s

T absolute temperature, K

T_s absolute temperature of reactive surface, K

T_g, T_{go} gas absolute temperature, gas temperature at time zero, K

T_w ,T_{wo} absolute temperature of substrate wall, wall temperature at time zero, K

T_{gin} absolute temperature of gas at inlet, K

W velocity component in z direction, parallel with substrate axis, m/s

X sequential number of the time step

x,y,z Cartesian co-ordinates

ε porosity fraction

φ parameter $hA_v / (\rho_w c_w)$, /s

ξ temperature ramp, K/s

ρ_g gas density, kg /m^3

ρ_s density of monolith wall material, kg /m^3

ρ_w substrate bulk density, $\rho_s (1 - \varepsilon)$ kg /m^3

1.0 INTRODUCTION

Automotive catalysts are an important means for pollution reduction. They do not, however, work at full efficiency until they reach the light-off temperature, in the region of 500K. Up until the time of light-off unconverted pollutants are expelled from the exhaust system to the atmosphere. Warm-up prior to light-off is important so that the catalyst reaches its operating temperature in as short a time as possible. A model of warm-up prior to light-off has been developed by the present authors **[1]** from studies of non-reactive catalyst substrates under steady flow conditions. The exhaust gas stream in a typical system is, however, pulsating at frequencies in the range up to 100 Hz. The effect of pulsating flow on velocity and mass flow distribution in catalyst systems is of particular interest. A poor distribution of mass flow can cause under utilisation of some parts of the catalyst and over utilisation of other parts, which may degrade and thereby reduce the overall lifetime of the catalyst. Pulsating flow also directly affects the warm-up of the catalyst by its influence on the convective heat transfer process **[2].**

Although the function of the exhaust catalyst has been much studied in recent years, many studies are modelling based and there is a dearth of data for validating the models. The simplest models have chemical schemes that consider only oxidation of CO and hydrocarbons; often the latter are represented by the single compound propene, C_3H_6. Such models aim to describe realistically the processes in the exhaust of lean burn engines with simple Pt catalysts. Models of this type were first developed about twenty years ago **[3]** and were amenable to numerical solution processes **[4]**. More recently, catalysts containing more than one precious metal and which reduce NOx simultaneously with oxidation of other pollutants have been developed and come into common use. These are generally referred to as three way catalysts. Those involved in modelling have incorporated the additional chemical reduction reaction, together with the oxidation of slow and fast hydrocarbons and the oxidation of hydrogen. Oxygen storage is also important when lambda excursions between rich and lean occur in the engine operation. Catalyst ageing is also included in some models, the mechanisms being either poisoning by, for example, phosphorous or sintering by excessive temperatures and other effects. There are other reactions that are known to occur in automotive catalysts but which are not yet generally included, for example water gas shift and steam reforming.

If models are to be useful for practical application they must be computationally efficient and provide validated results with minimal effort. Many of the models described in the literature are 1D and non-pulsating. Any attempt to fully model 2D geometries introduces flow field and thermal problems **[5],** which add unnecessary complexity for validating the reaction modelling. The present authors have previously considered 1D warm-up under pulsating flow conditions **[2, 6].** These studies under non-reacting conditions showed a very small effect of approximately sinusoidal pulsations on warm-up. This work has been extended to less idealised conditions on an engine test bed with non-sinusoidal pulsating flow. The data obtained were presented in an earlier paper **[7]**, which includes a brief review of the modelling approaches of other authors.

Warm-up of a variety of substrates to light-off by pulsating fuel-rich gasoline engine exhaust under 1D conditions **[7]** was studied both experimentally and via CFD simulations. This paper discusses a similar study but for the 2D case with lean exhaust. Although the literature on this subject is quite extensive, the majority of the work is simulation based. The work reported here, however, covers both measurements and CFD predictions and in particular examines the effect of flow pulsations. In the tests the temperature was ramped up rapidly in a

manner typical of a practical catalyst located close to the engine. The temperatures were measured to provide a thermal map of temperature distribution within the substrate, rather than solely gas temperatures at inlet and exit. The tests were performed on both non-reactive and reactive substrates and were designed to look at a range of substrate properties. Species concentrations were measured upstream and downstream of the catalyst. Nine different substrate types and two engine speeds were investigated. One of the substrates was a hybrid sample, with the front end non-reactive to simulate an aged catalyst. Warm-up of the non-reactive substrates by the pulsating exhaust from a four-cylinder gasoline engine provided data for assessing the ability of the model to predict temperature.

The CFD model discussed in this paper uses a simple oxidation only chemical model to make 2D predictions of both temperature and conversion. It is based on a porous medium approach, developed for predicting temperatures prior to light-off **[1]**. The ability of a model to predict light-off is dependent upon its ability to predict temperature prior to light-off and these are both addressed here. There is particular emphasis on the ability of the model to predict the onset of light-off when the mass flow is pulsating, as in real exhaust systems.

2.0 THEORY

2.1 Simple catalyst warm-up theory

The simple theory of catalyst warm-up has been developed by the present authors in two previous papers **[1, 6]** with particular reference to light-off time. A similar analysis is considered below to assess the influence on warm-up of a large difference between the inlet gas temperature and the initial wall temperature. The gas temperature at inlet can be defined as $T_{gin} = T_{go} + \xi t$ where ξ K/s is the ramp. Then the equation describing the warm-up of the substrate mass near the inlet plane is

$$\frac{dT_w}{dt} = \frac{hA_v}{\rho_w c_w}(T_{gin} - T_w) = \varphi(T_{go} + \xi t) - \varphi T_w \qquad (1)$$

The solution of this equation is

$$T_w = (T_{wo} - T_{go} + \xi) e^{-\varphi t} + \xi t + T_{go} - \frac{\xi}{\varphi} \qquad (2)$$

The rate of rise of wall temperature is given by (1) above, but differentiating (2) gives an alternative expression that reveals the significance of the quantities $(T_{go} - T_{wo})$ and ξ.

$$\frac{dT_w}{dt} = (T_{go} - T_{wo})\,\varphi\, e^{-\varphi t} + \xi\,(1 - e^{-\varphi t}) \qquad (3)$$

Three special cases can be considered:

(1) Constant $T_{gin} = T_{go}$, i.e $\xi = 0$

In this case, the second term in equation (3) is zero and dT_w/dt depends upon parameter φ and on the magnitude of $(T_{go} - T_{wo})$.

(2) Constant ramp ξ and $T_{go} = T_{wo}$

In this case, the first term in (3) is zero and the value of dT_w/dt is determined only by ξ and parameter φ.

(3) Constant ramp ξ but $T_{go} \neq T_{wo}$

In this case, from (3) the value of dT_w/dt depends upon $(T_{go} - T_{wo})$, ξ and parameter φ.

The warm-up of the substrate further downstream away from the inlet plane is governed by the relationship between the gas temperature gradient, the mass flow rate and the rate of rise of wall temperature with time **[1]**.

$$\frac{dT_g}{dz} \sim - \frac{\rho_w}{m'} \frac{dT_w}{dt} \qquad (4)$$

When the flow is pulsing, possibly with very small or reversed flows at some stages of the cycle, the inverse of the mass flow rate will have a series of values with time that precludes simple time averaging to ascertain the effect of the pulsating mass flow. Furthermore, looking at the special cases above, it is clear that if the value of either $(T_{go} - T_{wo})$ or ξ is very large, then the value of dT_w/dt will also be large in the early stages of warm-up and this will compound the effect of pulsating flow on substrate warm-up.

2.2 Oxidation chemical model

The chemical reaction scheme used was similar to that described in **[7]**. As the tests were lean, it was not necessary to include NOx reduction. Only the following oxidation reactions were modelled.

$2CO + O_2 = 2CO_2$ $\qquad \Delta H_{CO} = -283.0E+03$ J/mol

$2C_3H_6 + 9O_2 \quad = 6CO_2 + 6H_2O \qquad \Delta H_{C3H6} = -1926.3E+03$ J/mol

The reaction kinetics scheme is due to Oh and Cavendish **[3]** but was derived from the original scheme of Voltz et al. **[8]**. The reaction rate expressions are given below. The concentrations C_{CO} and C_{C3H6} are mol fractions of reactants in the vicinity of the noble metal surface

$$R_{CO} = A_c\, k_1\, C_{CO}\, C_{O2} / G \qquad [\text{mol s}^{-1}\text{ m}^{-3}] \qquad (5)$$

$$R_{C3H6} = A_c\, k_2\, C_{C3H6}\, C_{O2} / G \qquad [\text{mol s}^{-1}\text{ m}^{-3}] \qquad (6)$$

$$R_{O2} = 4.5\, R_{C3H6} + 0.5\, R_{CO} \qquad [\text{mol s}^{-1}\text{ m}^{-3}] \qquad (7)$$

The pre-exponential factors from the Voltz et al. scheme were re-presented by Oh and Cavendish as

$$k_1 = k_{CO} \exp(-E_{CO} / RT_s) \qquad [\text{mol K s}^{-1}\text{ m}^{-2}\text{ Pt}] \qquad (8)$$

$$k_2 = k_{C3H6} \exp(-E_{HC} / RT_s) \qquad [\text{mol K s}^{-1}\text{ m}^{-2}\text{ Pt}] \qquad (9)$$

where T_s K is the absolute temperature of the reactive surface.

The values for k_1 and k_2 require multiplication by a numerical value for the reactive surface area per unit volume (m^2 noble metal/m^3 monolith) in order to quantify the reaction rates. An A_c value of 27E+04 m^2/m^3, calculated from known precious metal loading and particle size, was found to be satisfactory for lean exhaust and fresh conditioned catalysts with no further multiplier required**.** The requirement for higher reaction rate constants for rich exhaust was discussed in **[7]**. The overall reaction rate determined from this scheme is the intrinsic chemical reaction rate, i.e. the effectiveness factor is taken to be unity; the rate calculated from these expressions does not therefore include any effects of species transfer by diffusion within the washcoat layer.

Because the frequency factors k_1 and k_2 are defined as above, the denominator G in the Oh and Cavendish scheme **[3]** includes the absolute temperature.

$$G = J_1\, J_2\, J_3\, T_s \qquad (10)$$

The effect of the terms J_1, J_2 and J_3 are discussed in the original paper by Voltz et al. **[8]**. They are inhibitors that reduce the reaction rate due to the chemisorption of CO and C_3H_6 and to the adsorption for NO respectively. Term J_2 improves the fit to experimental data at higher concentrations of CO and C_3H_6. The adsorption constants take the values given below. The term Z_1 is for CO, Z_2 for C_3H_6, Z_3 for the combined

effect of CO and C_3H_6 and Z_4 for NO. Although reduction of NO was not included in the model, the levels were monitored in the tests to provide values for this term.

$$J_1 = (1+ Z_1 C_{CO} + Z_2 C_{C3H6})^2 \quad (11)$$

$$J_2 = (1+ Z_3 C_{CO}^2 C_{C3H6}^2) \quad (12)$$

$$J_3 = (1+ Z_4 C_{NO}^{0.7}) \quad (13)$$

$$Z_1 = 65.5 \exp (961/T) \quad (14)$$

$$Z_2 = 2080 \exp (361/T) \quad (15)$$

$$Z_3 = 3.98 \exp (11611/T) \quad (16)$$

$$Z_4 = 4.79E+05 \exp (-3733/T) \quad (17)$$

This scheme outlined above **[3, 8]** is commonly used as the basis for exhaust catalyst modelling and was found to work well for the lean exhaust conditions in the tests described in this paper.

3.0 CFD METHODOLOGY

3.1 Basis of CFD model

The simple theory of warm-up discussed above examines some special cases; the general case is more fully described by the equations below that form the basis of the CFD model. The co-ordinate system is set up so that the substrate axis and flow are in +z direction. The thermal conduction equation for the substrate wall in a non-isotropic continuum, assuming cylindrical symmetry, is

$$\rho_s (1-\varepsilon) c_w \frac{\partial T_w}{\partial t} - k_{ax} \frac{\partial^2 T_w}{\partial z^2} - \frac{k_{rad}}{r} \left[\frac{\partial}{\partial r} \left(r \frac{\partial T_w}{\partial r} \right) \right] = -h A_v (T_w - T_g) \quad (18)$$

Assuming the flow is unidirectional through the substrate, the energy equation describing the gas is

$$\rho_g \varepsilon c_{pg} \left[\frac{\partial T_g}{\partial t} + W \frac{\partial T_g}{\partial z} \right] - \varepsilon k_g \frac{\partial^2 T_g}{\partial z^2} - \frac{\varepsilon k_g}{r} \left[\frac{\partial}{\partial r} \left(r \frac{\partial T_g}{\partial r} \right) \right] = -h A_v (T_g - T_w) \quad (19)$$

These two equations are simultaneous and there is continuity of heat flux at the boundary between the gas and the solid porous medium. When the equations are solved numerically, the heat transfer between the gas and the wall is dealt with as a source term calculated from known heat transfer coefficients. The quantity A_v (m^2/m^3) is

the effective bulk value of wetted area per unit volume available in the substrate. Values for this are determined from the substrate geometry and are indicated in Table 1.

The model considers two chemical species: CO and C_3H_6. Oxidation of CO and C_3H_6 does not generate any significant products in this simple chemical scheme and so the species are treated as passive scalars. Oxygen is included as a third species for monitoring purposes. The assumption is made that no reactions occur in the gaseous phase, only at the solid surface. The monolithic structure of the catalyst with separated channels ensures that there is transport of species by flow only in the *z* direction.

The simplified conservation equation for chemical species in the gaseous phase in the exhaust may be expressed, with diffusion neglected, as

$$\frac{\partial}{\partial t}(\rho_g C_{gi}) + \frac{\partial}{\partial z}(\rho_g W C_{gi}) = S \qquad (20)$$

The source term S describes transfer of species from solid to gas.

$$S = \rho_g K_{mi} A_v (C_{si} - C_{gi}) \qquad (21)$$

Since concentration mass fraction C_{si} will be less than concentration mass fraction C_{gi} the term S will be a species sink term for the gas cells in the model. Values for mass transfer coefficients K_{mi} and for A_v must be specified. The values for K_{mi} are dependent upon diffusion coefficient values, which change with temperature. Allowing the mass transfer coefficient to vary with temperature was found to have an insignificantly small effect on the prediction of light-off and so constant K_m values were used, namely 0.181 m/s for CO, 0.181 m/s for oxygen, 0.105 m/s for C_3H_6.

It is assumed that there is no accumulation of species in the solid phase so the concentration of species on the monolith surface is governed by

$$\rho_g K_{mi} A_v (C_{gi} - C_{si}) = M_i R_i \qquad (22)$$

where M_i is molar mass in kg/mol and R_i is reaction rate in the solid phase in mol/sec/m^3.

When catalytic reactions occur, equation (18) describing the solid has an extra source term due to the heat released through the chemical oxidation reactions in the solid phase.

$$S_e = R_i \, \Delta H_i \tag{23}$$

A full CFD model that includes the diffuser upstream of the substrate was used for comparison with the non-reactive test data. This additionally solved the momentum and continuity equations to establish the flow field in the diffuser. A smaller model of only the substrate was used for comparison with the reactive tests. Further details of the two models are given below. The CFD simulations were carried out by solving the above equations using the commercial CFD package Star-CD from Computational Dynamics Ltd. The source terms for heat transfer and species transfer between gas and solid phases were evaluated in user subroutines. The models were run on an SGI Indy Workstation with 256 MB RAM and R5000 processor.

3.2 Details of CFD model for non-reactive cases

The catalyst monolith is modelled as an analogous porous medium. In the CFD model, the porous medium cells are defined as fluid, but have resistance so that the velocity and pressure drop are modeled correctly. The porous medium fluid cells in Star-CD cannot, however, model the thermal behaviour of the channel walls. A second block of computational cells, defined as having solid properties, models the bulk of the monolith and wall temperature is solved for in these solid cells. Heat transfer between the block of porous medium fluid cells and the block of solid cells is carried out numerically within user-defined subroutines of the CFD code. In this way it is possible to model the catalyst monolith fully, but without the need to model individual channels, which is computationally prohibitive.

The wedge shaped mesh used for the 2D axially symmetric simulations is shown in Figure 1A. The axis of the model is the z-axis. The wedge angle is 5°. The inlet pipe is 60 mm long, with 24 mm radius and has a 2mm thick metallic wall. The cone is 60 mm long, and expands the duct from 24 mm radius to 59.2 mm. The cone has an approximately 2mm thick metallic wall. There is a 20 mm length of 59.2 mm radius duct prior to the substrate, also with a 2mm thick metallic wall. The flange is approximated by 25 cells that are assigned metallic

properties. The porous medium (fluid cell block) is 120 mm long and has radius 59.2 mm. The outlet duct is 60 mm long, also with 59.2 mm radius, but its metal wall is not modelled. The bulk substrate is modelled by a block of solid cells with the same dimensions as the porous medium. The 2mm thick mantle is modelled by a two-cell layer on the solid cell block and the flange is approximated by 30 cells. The pressure loss entrance-effect correction **[9, 10]** was included in the simulations, as discussed below. Measured temperature data for the substrate prior to the start of the experiment were used to initialise the model.

The CFD simulations were run for steady and pulsating flow, in both cases thermally transient using the PISO **[11]** algorithm. For steady flow the time step was 0.005 seconds. Runs for 35 s of warming required 7000 time steps and took about 24 hours. Runs for 60 s warming required 12000 time steps and took about 48 hours. The cells in the 48 mm diameter inlet duct were 4 mm long. The velocity corresponding to 30 g/s was 13.8 m/s cold, 41.4 m/s at about 900 K. The minimum cell residence time was thus 0.000097 s and so a time step of 0.005 satisfies the Courant number criterion **[12]**, $\Delta t \leq 50\ t_r$ in all parts of the model throughout the warm-up simulation. For pulsing flow, the time step was set smaller, either at 0.0005 secs (35 secs in 70,000 time steps) or at 0.00025 secs (20 secs in 80,000 time steps).

The RNG version of the standard k-ε turbulence model was used to model the flow in the inlet pipe and diffuser. Upwind differencing was used for all parameters except density, which was solved with central differencing. At inlet, a turbulence intensity of 2% and length scale of 10 mm was specified.

Figure 2 shows some cold flow radial velocity profile predictions from the non-reactive 2D model at exit from the monolith. These were done for 0.0297 kg/s mean mass flow rate and for the properties of a washcoated ceramic monolith. They show that the predicted velocity profiles are flattest for steady flow and most maldistributed for the simulated engine pulsations that are discussed later in Section 5.2. The frequency of the sinusoidal and engine pulsations was 100 Hz. The amplitude of the sinusoidal pulses was 85% of the mean flow rate. In each case, inclusion of the pressure loss entrance effect **[9, 10]** in the model increases the predicted maldistribution. The plots in Figure 2 typify the tendency of CFD simulations to predict increased flow maldistribution with pulsations. This contradicts experimental observations that indisputably show flatter velocity profiles with pulsating flow at frequencies in the region of 100 Hz. **[10, 13]**. The predicted profiles shown in Figure 2, however, will change with temperature.

Figure 3 shows the predicted mass flow profiles 9 mm downstream of the substrate exit for another case under steady flow conditions. This case examined the 400/2 metallic substrate. The simulations were again carried out both with and without the pressure loss entrance effect. Values of $\rho_g W$, mass flow per unit area, relative to the mean mass flow per unit area are plotted. The profiles can be seen to feature the familiar maldistributed shape (compare with Figure 2 for the ceramic substrate) and also illustrate the redistribution of mass flow that is predicted to occur with rise in temperature. The predicted flow profile is flatter near the axis of the substrate (depth D, 59.2 mm) at higher temperature and the difference between predictions with and without the entrance effect is smaller at 35 secs when the temperature is higher. This suggests that it may be acceptable to assume flat velocity profiles in a warming substrate.

3.3 Details of CFD model for reactive cases

The wedge shaped mesh used for the 2D axially symmetric reactive simulations modelled the porous medium brick only, see Figure 1B. This was thus a much smaller model than the one shown in Figure 1A. The axis of the small model is the *z* axis and the wedge angle is 5° as in the larger model. A short inlet fluid duct section of 20 mm length and 118.4 mm diameter is modelled upstream of the substrate. The substrate has length 120 mm and diameter 118.4 mm. The outlet fluid duct is 20 mm long. The substrate is modelled by a solid block with the same dimensions as the porous medium. The 2mm thick mantle is modelled by a two-cell layer.

As in the non-reactive studies, it was necessary to initialise the temperature field in the substrate in each case separately. The inlet boundary was immediately upstream of the substrate, and it was necessary to input both mass flow and temperature here. When the flow is steady, the maldistribution caused by a conical diffuser can result in, at worst, a 3:1 ratio between the highest and lowest local mass flow rates through the substrate. A mass flow rate change of this order has per se only a small effect on predicted light-off time, **[7]**. A paper published by the present authors et al. **[10]** shows experimental data that indicate that for 100 Hz pulsations in mass flow, and for Re less than 50,000, the velocity profile for a 60 ° diffuser is, however, approximately flat. It was therefore decided to run the reactive CFD model for a flat mass flow profile at the model inlet boundary, since small deviations from such a profile would have only a small effect on predicted light-off time. Another reason for this choice was the fact that CFD predicted mass flow profiles were found to be flatter as temperature rises (Figure 3). Also, practical simulation time issues encouraged the use of a reduced model size together with a flat

flow profile at the inlet boundary. Non-reactive steady-flow full-model CFD simulations had shown that the gas temperature on the axis at the substrate inlet face was the same as the gas temperature in the supply pipe upstream of the cone. There was, however, an approximately linear fall off of temperature from the axis to the cooler outer wall. This fall off was found in each case for a comparable non-reactive simulation and was in the range 60 to 100 K. This information was used to supply the temperature at the inlet boundary to the CFD model.

The CFD simulations were run transient using the PISO **[11]** algorithm. The cells in the porous medium were 4 mm long. The velocity corresponding to 30 g/s was 2.3 m/s cold, 6.8 m/s at about 900 K. The minimum cell residence time was thus 0.6 ms for which a time step of 0.03 s would meet the Courant number criterion **[12]** $\Delta t \leq 50\ t_r$ in all parts of the model. In fact, a shorter time step of 0.01 s was used. Runs for 30s of warming required 3000 time steps and took between 16 and 36 hours, dependent upon the case.

4.0 EXPERIMENTAL METHOD

The 2D tests were carried out in an engine test cell on a 1.6 litre Ford Sigma engine with a modified exhaust system. A schematic diagram of the test rig is shown in Figure 4. The inlet pipe to the diffuser was 48 mm in diameter. The conical diffuser expanded up to about 120 mm in diameter (allowing for the mantle or mat on the outside of the substrate) over a 60 mm length. Thus the diffuser included angle was 60 ° approximately. There was a 20 mm length of straight duct between the cone and inlet face of the catalyst substrate.

The substrates were 120 mm in length and 118.4 mm in diameter. The washcoat loading was 2.4 ± 0.15 g/in^3 (153 kg/m^3 approx.). The hybrid sample was washcoated but the front 1/3 was non-reactive (40 mm length) and the rear 2/3 was reactive (80 mm length). The reactive substrates for tests were loaded at 100g/ft^3 (3.53 kg/m^3) with a blend of Pt/Rh in the ratio 14:1. The hybrid sample was loaded at the rate of 40 g/ft^3 (1.412 kg/m^3) with a blend of Pt/Rh in the ratio 5: 1. The aim was to coat only half of the brick with precious metal, although the staining of the washcoat suggested that closer to 2/3 of the brick was treated.

The thermocouple holes in all the substrates were 35, 50, 70 and 85 mm from the inlet face. The holes were drilled so that the thermocouple tips would lie at depths, D, of 15, 30, 45 and 50 mm. The holes were drilled manually in the ceramic samples but were laser drilled in the metallics, with the consequence that the depths

were achieved less precisely in the metallics, and hence have slightly different values. Both non-reactive and reactive tests were carried out on the same test rig under approximately the same engine conditions.

The engine test procedure consisted of the following steps.

(1) New catalyst conditioning cycle: the catalyst valve was opened and the engine was run until the temperature at all the thermocouples within the substrate exceeded 700 °C (973 K). This condition was maintained for 30 minutes and the engine was then stopped and the rig cooled

(2) Test pre-conditioning cycle: the engine was started and run to achieve the specified operating conditions for the specific test whilst warming the catalyst. When the temperature at all the catalyst thermocouples exceeded 200 °C (473 K), the by-pass valve was opened and the catalyst was allowed to cool. Ideally the engine continued to run, exhausting through the by-pass during this period. If the catalyst did not cool, the engine settings were saved, the engine was stopped and then only restarted after the catalyst had cooled.

(3) Once the minimum catalyst temperature reached 120 °C (393 K) , and the engine operation was stable, the test was started by opening the catalyst valve. This temperature is below the anticipated light-off temperature but high enough to ensure absence of condensed water from the substrates. In practice, some difficulty was experienced in cooling the catalyst after the pre-test cycle, even with external fans. Consequently, when the catalyst minimum temperature had fallen to 393 K as required, parts of the substrate remained at higher temperatures.

(4) The test was run until the catalyst was fully warmed up in the case of the non-reactive samples so that the exhaust gas outlet temperature was close to the inlet temperature. In the case of the reactive samples, the test was run until the catalyst had lit off.

(5) The engine was shut down and the rig was cooled. The test continued at step 2 for a further test on the same substrate or at step 1 for a test on a different sample.

An aim for the tests was to vary engine speed (i.e. rpm and frequency) between tests but to fix mass flow rate by changing the engine load. The target operating conditions were:

0.02 kg/s total mass flow; 2000 rpm; 16/1 air/fuel ratio

0.02 kg/s total mass flow; 3000 rpm; 16/1 air/fuel ratio

0.03 kg/s total mass flow; 3000 rpm; 16/1 air/fuel ratio

The non-reactive testing programme encompassed five tests, see Table 2. The reactive testing programme investigated a larger number of conditions but five typical tests are listed in Table 3. The species concentrations at inlet were monitored in the engine tests and the mass fractions were as in Table 3. The concentrations of CO, hydrocarbons, NOx and O_2 were measured upstream and downstream of the catalyst using calibrated Horiba gas analysers. The concentration of hydrocarbons was also measured both upstream and downstream using calibrated Cambustion Fast Flame Ionisation Detectors (FFIDs). The response time of the FFIDs, nominally 4 ms, was very much faster than the Horiba analysers. The Horiba analysers were reliable for measuring the approximately constant exhaust concentration immediately downstream of the engine. Their response time, however, when supplied via narrow bore sampling tubes was not fast enough to properly monitor the conversion of species through light-off. The results obtained, discussed later, confirm and demonstrate this.

5.0 RESULTS

5.1 Results of engine tests compared with steady flow CFD simulations for non-reactive cases

The results for Test 355 are presented in detail here. These were for the non-reactive 400/2 metallic sample. Figure 5 shows the temperature rise with time, measured and predicted, in the substrate at depths D of 15 mm and 55 mm approximately. The variation from the prescribed depths in the data is due to the variation in hole depths achieved by laser drilling of this metallic sample. Agreement is seen to be very good. Deep in the substrate near the axis the measured temperatures are seen to be below the predicted temperatures at later times. At the shallower depth, the measured temperatures are seen to be higher than predicted. These results are typical of observations with all the different substrates.

Figure 6 shows the gas temperature profiles predicted inside the diffuser cone 1 mm upstream of the substrate inlet face. This Figure also shows, for reference, the measured inlet values of the gas temperature in the 48 mm diameter pipe upstream of the diffuser cone. It can be seen that near the axis (at depth D 59.2 mm) the gas temperature at entry to the substrate is predicted to be the same as the value measured in the inlet pipe. Just upstream of the substrate there is a significant temperature fall-off towards the cooler outer wall. The fall off is of order of 100 K in the simulation for Test 355 shown in Figure 6. This predicted fall off from the non-reactive

simulations was used for providing inlet temperature conditions in the reactive simulations; this is discussed further below.

The CFD simulations in Figure 5 included the pressure loss entrance effect. This is known from other steady flow studies to improve the agreement between measured and predicted velocity profiles **[9, 10].** Figure 7 shows predicted temperature profiles from the simulations carried out for Test 355 with and without the entrance effect. It shows the extent to which the CFD predictions of temperature are modified in this case. These predicted temperature profiles, for the substrate at *z* 35 mm, show that the influence of the entrance effect, which modifies the mass flow profile, is quite small. The predominant influence on the temperature profiles seen in Figure 7 is the temperature profile upstream of the substrate, Figure 6, rather than the mass flow, Figure 3. This also may be partly explained by the fact that the influence of the entrance effect on mass flow profile is less pronounced as temperature rises (see Figure 3).

5.2 Results of engine tests compared with pulsating flow CFD simulations runs for non-reactive case

Test 355, discussed above as a steady flow study, has also been run as a 2D pulsing flow study. A one-dimensional engine simulation code provided the 'wave' shape of the exhaust pulse for the Ford engine used in the tests. Figure 8 shows the pulse shape corresponding to a mean mass flow rate of 0.0297 kg/s. It can be seen that the pulse shape from a firing engine is far from being approximately sinusoidal. The engine pulse shape is complex with reversed flow in part of the cycle. Four pulses of approximately this shape are fed to the catalyst per 2 revolutions (720° crankshaft angle). The CFD model has also been run for the hypothetical idealised sinusoidal mass flow input:

$M = 0.0297 + (P/100) * 0.0297 * \sin(2 \pi X / N)$ kg/s

where amplitude is *P*% of mean, *X* is the time step number and *N* is the number of time steps per cycle. The CFD model was run for *P* set at 85 % and *N* set at 40, so that the time step is 0.00025 s for frequency 100 Hz. These simulations, together with a comparative steady flow simulation, were run with the pressure drop entrance effect.

The velocity in the inlet duct corresponding to the peak mass flow rate of 105 g/s was 48.0 m/s cold and 145 m/s at about 900 K. The minimum cell residence time was thus 0.000028 s. The time step of 0.00025 s, necessary to

characterise the inlet pulse shape, is well below the Courant number criterion **[12]**, $\Delta t \leq 50\ t_r$ in all parts of the model.

The results from the full CFD model including the diffuser cone are shown in Figures 9 and 10. The predictions are discussed first. In these figures 'sine' indicates sinusoidal pulses, 'wave' indicates the simulated engine pulse shape and 'steady' indicates non-pulsing flow. It can be seen that the steady flow is predicted to be best for warming the substrate, that the sinusoidal pulses are less effective and that the simulated engine pulses are least effective. This is most noticeable in Figure 9 at 15 secs for *z* 35 and *z* 50 mm, i.e., at the front end of the catalyst. Changes in the mass flow distribution that are predicted between steady and pulsing flow, Figure 2, that could change the temperature profile shape are masked by the effect of the pulsations. The predicted velocity distributions would imply that pulsing flow would lead to higher temperatures near the axis, but in fact near the axis they are generally lower than for steady flow. Figure 10 shows how the differences in predictions become greater at later times. In the very early stages of warm-up, the pulsating flow can be more effective towards the rear of the catalyst but this advantage is lost at later times. The differences between steady and sinusoidally pulsing flow are predicted to be small but the differences between pulsing flow from an engine and steady flow are predicted to be greater. Previous work **[6, 7]** has tended to suggest a minimal effect of pulsations on CFD predictions. The case discussed here, however, differs in that the incoming gas temperature at the start of the experiment is about 300 K hotter than the substrate. Within 5 seconds the gas has reached a constant temperature in the region of 950 K. This large difference between gas and substrate temperature amplifies the changes in the predictions caused by the mass flow pulsations, as discussed in the simple warm-up theory in section 2.1 above. Previously considered cases **[7]** had slow temperature ramps with the incoming gas temperature being initially lower than the substrate temperature. The cases discussed in this paper also differ in that the engine pulse shape is not approximately sinusoidal; the peak mass flow in Figure 8 has a value between three and four times the cycle averaged mass flow value.

Figure 9 also shows how the CFD predictions for Test 355 compare with the data. There is scatter in the data from the engine test, but Figure 9 shows improved agreement of data with the pulsing flow simulation for the simulated engine pulse shape. This is apparent throughout the substrate, from *z* 35 mm to *z* 85 mm.

5.3 Results of complementary 1D simulations

Some 1D simulations using a porous medium model consisting of a line of single cells **[6]** were carried out to confirm the effect of pulse shape on the predicted temperature. The two pulse shapes shown in Figure 8, the simulated wave from the engine and the sinusoidal pulse shape, were investigated, together with steady flow. An extreme pulse shape, which can be envisaged as a series of shots of mass flow, was also investigated. This 'shot' pulse shape was a mass flow rate equivalent to 0.005 kg/s for the first 32 time steps of every 40 time step cycle, then of 0.252 kg/s for steps 33 to 36, and then of 0.005 kg/s for steps 37 to 40. The mean flow was thus 0.0297 kg/s as in the other cases. The inlet temperature was constant at 950 K and the initial temperature was 400 K. These CFD predictions were checked by running some 200 time step/cycle simulations, which gave identical values to the 40 step/cycle simulations.

The results of these simulations are shown in Figure 11 where a very clear effect of pulse shape can be seen. Previous studies **[6, 7]** have shown that the predicted effect of pulsations is small when the inlet gas temperature ramp is slow, 20 K/s or less and the initial inlet gas temperature is approximately the same as the initial substrate temperature. In this case, however, where there is a large difference between the gas and wall temperatures at the start of the experiment, the effect of pulsations is significant. Furthermore the nature of the pulse shape is also influential. The experimental conditions prevailing in the engine tests are pulsating flow together with a large value of (T_{go}-T_{wo}). These are responsible for the effect demonstrated in Figure 11 being seen in Figures 9 and 10. The very strong effect of pulsations (Figure 11) is not countered by the predicted mass flow distribution (Figure 2).

5.4 Results of engine tests compared with CFD simulations for reactive cases

The results for two cases are presented here. These are Test 330, for the hybrid sample that approximates to an aged catalyst and Test 343, for the 800/2 metallic. Steady flow CFD simulations of warm-up through light-off are compared with temperature and conversion data obtained under pulsating conditions. Flat velocity profiles at the inlet boundary just upstream of the substrate were justified for three reasons. Mass flow per se has little effect on light-off time **[7]**. Experimental observations have shown flat velocity profiles at mass flow pulsation

frequencies of 64 and 100 Hz **[13]**. Use of the correct temperature profile upstream of the substrate at the inlet boundary, Figure 6, is more important than deviations of mass flow from a flat profile, which in any case are predicted to become less as the temperature rises.

5.4.1 Results for the hybrid sample

Test 330 was a test on the hybrid sample, which had the front third of its length non-reactive. In the CFD simulation *Ac* was set to zero for the first 40 mm length and was set to 27E+04 m^2/m^3 for the remainder. Figure 12 shows the initial temperature distribution within the substrate prior to the start of the experiment. This information was used to specify the initial condition for the CFD simulation. This was done for every test individually as the initial state of the substrate was very different in each case. The temperature fall off from axis to outer wall at the substrate inlet face was estimated to be 80 K throughout the simulation, based on a non-reactive full simulation including the diffuser cone. Uniform mass flow was assumed as the pulsing frequency was 100 Hz. The inlet species concentrations were as listed in Table 3.

Figure 13 shows the solid wall temperatures predicted by steady flow CFD compared with observed data. The four graphs relate to planes at *z* 35, 50, 70 and 85 mm from the inlet face. On each graph results at different depths, D, are indicated. Overall agreement is very good. Figures 14 and 15A show predicted conversion compared with observed data. The CFD predictions show that light-off time is predicted to be very similar at a shallow depth and near the axis. The FFID data for hydrocarbons agree very well with predictions. The Horiba data show a significant delay compared with the FFID data; this can be attributed to the gas analyser system response time, which is of order s, whereas the FFID response is of order ms. The hybrid sample mimics an aged catalyst but light-off is seen to occur fairly rapidly with 50% conversion within 15 s from the start of the experiment. Figure 15A shows that light-off occurs when the front inactive part of the catalyst has reached a fairly high temperature, about 550 K. Figure 15B shows a similar plot but against temperature at *z* 70 mm, which is 30 mm into the active part of the catalyst. The light-off temperature is near to 450 K, which is a low value and characteristic of highly oxidising mixtures. Temperatures nearer 500 K were observed with rich mixtures **[7]**.

5.4.2 Results for Test 343

The temperature fall off from axis to outer wall at the substrate inlet face was estimated to be 100 K throughout the simulation in this case, based on a non-reactive full simulation including the diffuser cone. Uniform mass flow was assumed as the pulsing frequency was 100 Hz. The inlet species concentrations were as tabulated in Table 3.

Test 343 was carried out on the 800/2 metallic sample, which was expected to respond rapidly to warming. Figure 16 shows substrate temperatures as a function of time at different depths and axial locations. Overall, there is fair agreement between data and predictions, with fairly good agreement at the z 35 and 50 mm locations. Figure 17 shows conversion through light-off, both measured data and CFD predictions. The FFID data show that the conversion is very rapid in this case. This is attributable to two facts: the substrate was warm before the experiment started and this thin walled metallic substrate responds rapidly to warming. In the engine tests, although starting an experiment did occupy a finite time, mechanical operation of valves was estimated to have taken not more than 1 second.

Figures 17 and 18 show that the rapid conversion is predicted to be similar on the axis and at depth, D, 5.2 mm. Agreement of the FFID conversion measured curve with predictions is very good. The effect on observed data of the difference in response time of the FFID and Horiba analysers is again apparent. Figure 18 shows that light-off is predicted to occur at a low substrate temperature, in the region of 425K, which is consistent with chemical reactions in lean exhaust. Higher temperatures were noted in tests on rich exhaust **[7]**.

The general agreement of measurements with predictions was found to be remarkably good in all the cases investigated and this was achieved using a very simple, substrate only, model. The model included the assumption that the mass flow profile at the substrate inlet was flat, justifiable because the flow was pulsating at a frequency in excess of 60 Hz, but the model accounted for the non uniform temperature profile at substrate inlet.

6.0 CONCLUSIONS

Fairly good agreement was achieved between measured and predicted temperatures in non-reactive substrate tests by using steady flow in the CFD simulations. Better agreement was achieved when pulsating flow was included in the simulations. Forty time steps per cycle were found to be adequate for characterising the pulsations. Previous work had suggested that it was not necessary to include pulsations in simulations in order to make adequate temperature predictions, but these studies with simulated engine wave pulse shapes and with large difference between gas and wall temperature have shown that including pulsations in mass flow does change and improve the predictions. The effect of the pulsations is small when the temperature ramp at inlet is small and the initial temperatures of the gas and substrate are similar. If the inlet gas temperature is much warmer than the initial substrate temperature, the effect of pulsating mass flow is predicted to be significant. Simulations imply that steady flow is best for warming the substrate with sinusoidal pulses less effective. Simulated engine pulse shapes are even less effective, and 1D simulations have suggested that trains of isolated pulses of high mass flow rate and short duration are least effective. The effect of the pulsations surpasses the effect of the mass flow distribution that is present due to the diffuser cone.

For reactive substrates, steady flow CFD predictions for temperature and conversion agree very well with data obtained under pulsating flow conditions. This offers savings in computation time when simulating pulsating flow reactive cases. The reactive model used in these studies is a substrate only model and relies on correct mass flow and temperature data at the substrate inlet face. For high frequency pulsations, near 100 Hz, the flow profile is assumed to be approximately flat. This assumption is based on experimental evidence **[10, 13]** rather than CFD simulations, which are known to predict the mass flow profile incorrectly under pulsating conditions. The inlet temperature data for the reactive model simulations were based on separate full model non-reactive simulations. For lower pulsation frequencies, flow maldistribution information would need to be input to the substrate inlet for accurate predictions. Agreement between measurements and CFD predictions was achieved by using reaction rate constants based on the Oh and Cavendish **[3]** version of the kinetic scheme, attributed to Voltz et al. **[8]**, together with an *Ac* value of 27E+04 m^2/m^3 and without further multipliers. This seems to provide an adequate description of the reactions under lean conditions. The higher reaction rate constants and arbitrary multiplier used in the simulations of the 1D tests under rich conditions **[7]** were not required.

The results show that the models predict temperature quite well overall for both the non-reactive and reactive cases. Generally, conversion is correctly predicted if temperature is correctly predicted, and in these tests both

are described well by the model. Agreement noted between measurements and predictions is found to be equally good over the whole range of types of substrate investigated. The behaviour of the hybrid sample that simulated an aged catalyst was accurately predicted by a simple adjustment of the parameter A_c. The modelling approach has thus been found to be valid for a range of practical catalyst substrates.

7.0 ACKNOWLEDGEMENTS

The authors acknowledge ArvinMeritor Ltd., Ford Motor Company, Jaguar Cars Ltd., and Johnson Matthey plc; the project was supported under the SERC-DTI Link Programme on Applied Catalysis, which funded the research project.

8.0 REFERENCES

[1] Benjamin, S. F. and Roberts, C. A. Modelling warm-up of an automotive catalyst substrate using the equivalent continuum approach. *Int J Vehicle Design*, 1999, 22, 253 – 273

[2] Benjamin, S. F. and Roberts, C. A. Warm-up of an automotive catalyst substrate by pulsating flow: a single channel modelling approach. *Int J Heat and Fluid Flow*, 2000, **21**, 717 - 726

[3] Oh, S. E. and Cavendish, J. C. Transients of monolithic catalytic converters: Response to step changes in feedstream temperature as related to controlling automobile emissions. *Ind Eng Chem Prod Res Dev*, 1982, **21**, 29 - 37

[4] Fueyo, N. 1D simulation of a catalytic converter for cars. *Phoenics demonstration report*, PDR/CFDU/IC/35, CHAM Ltd. , 1987

[5] McCullough, G., Douglas, R., Cunningham., G., and Foley, L. The development and validation of a two-dimensional transient catalyst model for direct injection two-stroke applications. *Proc Instn Mech Engrs*, 2001, **215 (**Part D), 919 - 955

[6] Benjamin, S. F. and Roberts, C. A. Warming automotive catalysts with pulsating flows. *Proc Instn Mech Engrs, 2001,* **215** (Part D), 891 – 910

[7] Benjamin, S. F. and Roberts, C. A. Automotive catalyst warm-up to light-off by pulsating engine exhaust. Submitted to *Int J Eng Res*, 2002

[8] Voltz, S. E., Morgan, C. R., Liederman, D. and Jacob, S. M. Kinetic study of carbon monoxide and propylene oxidation on platinum catalysts. *Ind Eng Chem Prod Res Dev,* 1973, **12**, 294 – 301

[9] Benjamin, S. F., Haimad, N., Roberts, C. A. and Wollin, J. Modelling the flow distribution through automotive catalytic converters. *Proc Instn Mech Engrs,* 2001, **215** (Part C), 379 – 383

[10] Benjamin, S. F., Roberts, C. A. and Wollin, J. A study of the effect of flow pulsations on the flow distribution within ceramic contoured catalyst substrates. SAE Paper 2001-01-1996. Published in *General Emissions Research and Development, 2001,* **SP-1631**

[11] Issa, R. I. Solution of the implicitly discretised fluid flow equations by operator splitting. *J Comput Physics,* 1986, **62**, 40 – 65

[12] Computational Dynamics Limited. *Star-CD Users Guide, 1998.*

[13] Benjamin, S. F., Roberts, C. A. and Wollin, J. A study of pulsating flow in automotive catalyst systems. *Experiments in Fluids*, 2002, **33**, 629 - 639

TABLES (CAPTIONS ARE LISTED OVERLEAF)

Table 1

Property	400/6.5 Ceramic	600/4 Ceramic	400/2 Metallic	800/2 Metallic
Wall thickness	6.5 thou; 0.1651 mm	4 thou; 0.11 mm	0.05 mm	0.03 mm
Porosity %	67.1	68.8	77.97	79.57
Bulk density ρ_w kg/m^3	563	533	918	802
Sp Heat c_w J/(kgK)	914	914	567	578
A_v m^2/m^3	2579	3199	3140	4270
d_h mm	1.04	0.86	0.995	0.744
k [axial] W/(mK)	0.36	0.30	1.4	1.2
k [radial] W/(mK)	0.27	0.21	0.40	0.34
Permeability coeff α*	0.0001	0.0001	18.95	18.2
Permeability coeff β*	714	1018	460	805
Nu No.	3.608	3.608	2.4	2.7
h Av/(ρ_w c_w)	0.46	0.72	0.38	0.88

Table 2

Ref. No.	Substrate	Wall	Material	Total flow kg/s	Re approx.	Speed rpm	Air/Fuel
Test 350	400/6.5	0.165 mm	Ceramic	0.020	29150	2000	15.64
Test 352	400/6.5	0.165 mm	Ceramic	0.030	43725	3000	15.71
Test 320	600/4	0.11 mm	Ceramic	0.0199	29150	3000	15.90
Test 353	800/2	0.03 mm	Metallic	0.020	29150	2000	15.23
Test 355	400/2	0.05mm	Metallic	0.0297	43725	3000	15.85

Table 3

Test No.	Cat. type	Engine speed rpm	Total mass flow kg/s	CO Inlet mass fraction	HC Inlet mass fraction	NOx Inlet mass fraction	O_2 Inlet mass fraction	Air /Fuel ratio	Maximum initial substrate temp °C
330	Hybrid	3000	0.0202	0.00145	0.00083	0.00109	0.0243	14.91	200
336	600/4 ceramic	3000	0.0200	0.00111	0.000653	0.00109	0.0232	15.03	160
343	800/2 metallic	3000	0.01996	0.001064	0.000713	0.000756	0.0224	15.58	155
345	400/2 metallic	3000	0.0202	0.00116	0.000677	0.00109	0.0232	15.61	170
347	400/6.5 ceramic	2000	0.0203	0.00097	0.000592	0.00109	0.0232	15.64	170

TABLE CAPTIONS

Table 1 Properties of washcoated substrates
* The permeability coefficients quoted are for cold flow, but can be calculated as a function of temperature in the model.

Table 2 Engine tests of non-reactive substrates

Table 3 Engine tests of reactive substrates

FIGURE CAPTIONS

Figure 1A

Mesh for 2D axially symmetric non-reactive model with the two parts of the model shown. The fluid model, on the left, has solid inlet pipe wall 2 cells thick, solid cone wall 2 cells thick and attached flange 5 cells by 5 cells. The substrate model on the right has mantle 2 cells thick and flange 5 cells by 6 cells.

Figure 1B

Mesh for 2D axially symmetric reactive model with the two parts of the model shown. This model excludes the diffuser.

Figure 2

Radial profile of cycle-averaged velocity predicted by CFD for different pulse shapes with and without inclusion of the pressure loss entrance effect. Outer wall of monolith is at depth, D, 0 mm and axis at depth, D, 59.2 mm.

Figure 3

Predicted radial mass flow profiles for steady flow 9 mm beyond substrate exit at start and end of warm-up. Outer wall of monolith at depth, D, 0 mm and axis at depth, D, 59.2 mm.

Figure 4

Schematic diagram of engine test rig.

Figure 5

Comparison of steady flow CFD predictions, including the pressure loss entrance effect, with solid temperature data for engine Test 355 on 400/2 non-reactive metallic sample.

Figure 6

Predicted gas temperature profiles 1 mm upstream of substrate inlet face compared with measured gas inlet temperatures upstream of diffuser cone. CFD predictions are for steady flow including the pressure loss entrance effect.

Figure 7

The effect of the inclusion of the entrance effect on steady flow CFD simulations of temperature.

Figure 8

Simulated pulse from engine compared with hypothetical sine wave pulse.

Figure 9

Comparison of data for Test 355 with steady and pulsating flow CFD predictions.

[sine = sinusoidal pulse, steady = steady flow, wave = simulated engine pulse]

Figure 10

Steady and pulsating flow CFD predictions for Test 355 at two different depths.

[sine = sinusoidal pulse, steady = steady flow, wave = simulated engine pulse]

Figure 11

Results of 1D simulation of warm-up of 400 K substrate by 950 K gas, by steady flow and by three different pulse shapes (sinusoidal, engine pulse wave simulation, series of isolated pulse shots).

Figure 12

Initial temperature distribution in substrate for Test 330.

Figure 13

Measured temperatures compared with CFD predictions for Test 330.

[Lines are CFD simulations; Symbols are experimental data]

Figure 14

Comparison of measured conversion fraction with CFD predictions for Test 330 through light-off.

Figure 15

Comparison of measured conversion fraction with CFD predictions for Test 330 plotted as a function of substrate temperature at [A] *z* 35 mm and [B] *z* 70 mm.

Figure 16

Measured temperatures compared with CFD predictions for Test 343

[Lines are CFD simulations; Symbols are experimental data]

Figure 17

Comparison of measured conversion fraction with CFD predictions for Test 343 through light-off.

Figure 18

Comparison of measured conversion fraction with CFD predictions for Test 330 plotted as a function of substrate temperature at *z* 35 mm.

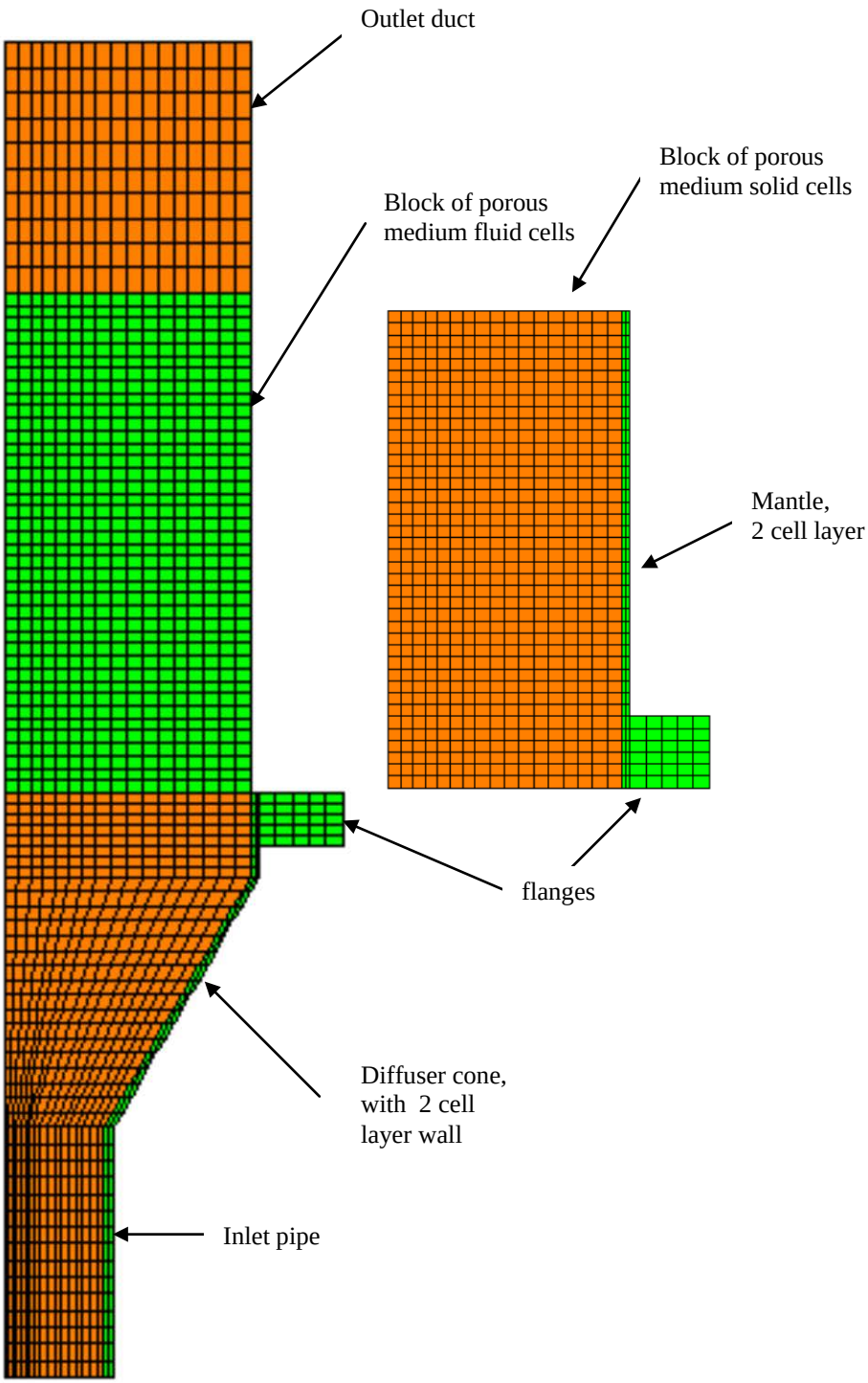
Outlet duct
Block of porous medium solid cells
Block of porous medium fluid cells
Mantle, 2 cell layer
flanges
Diffuser cone, with 2 cell layer wall
Inlet pipe

Figure 1A

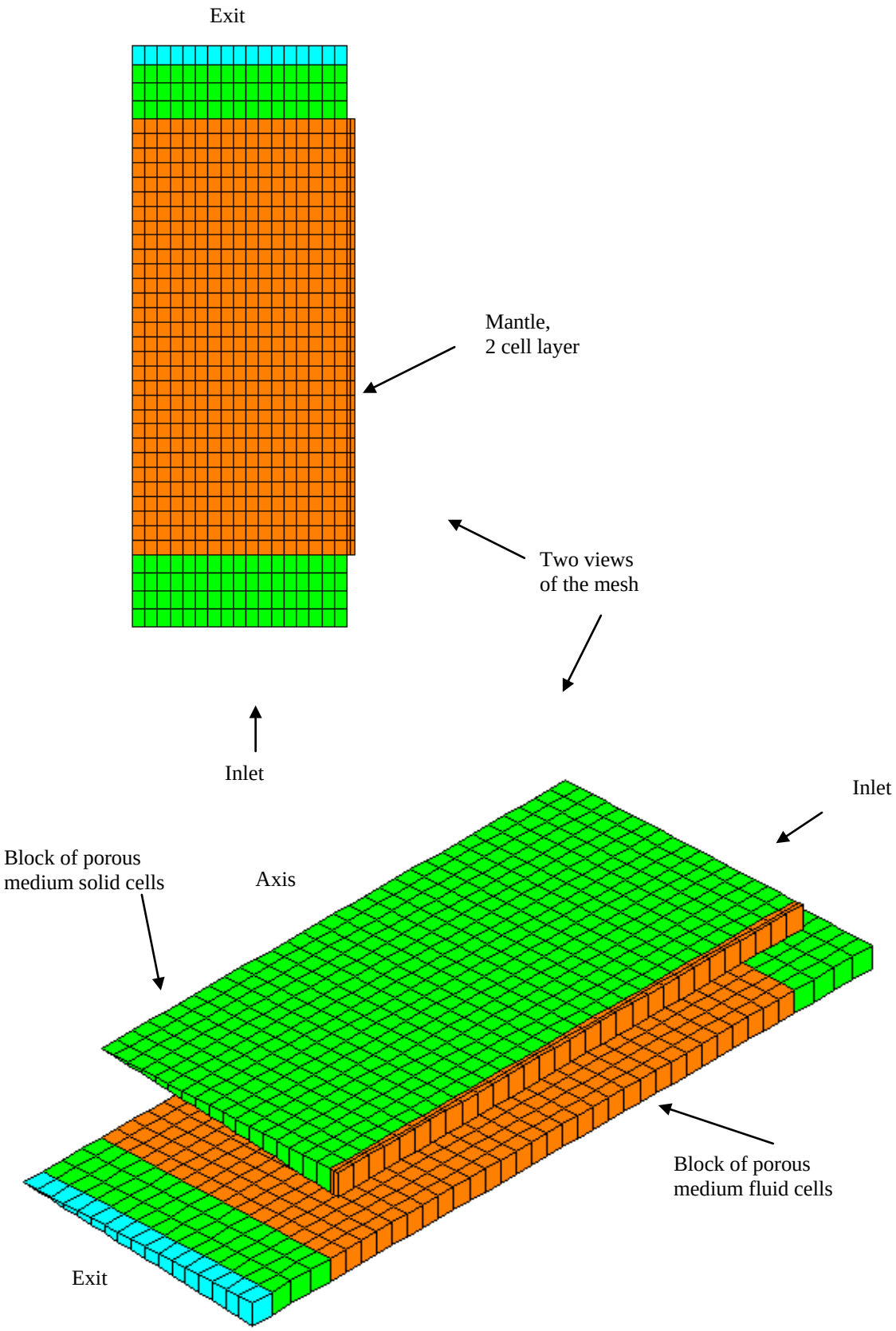
Exit
Mantle,
2 cell layer
Two views
of the mesh
Inlet
Inlet
Block of porous
medium solid cells
Axis
Block of porous
medium fluid cells
Exit

Figure 1B

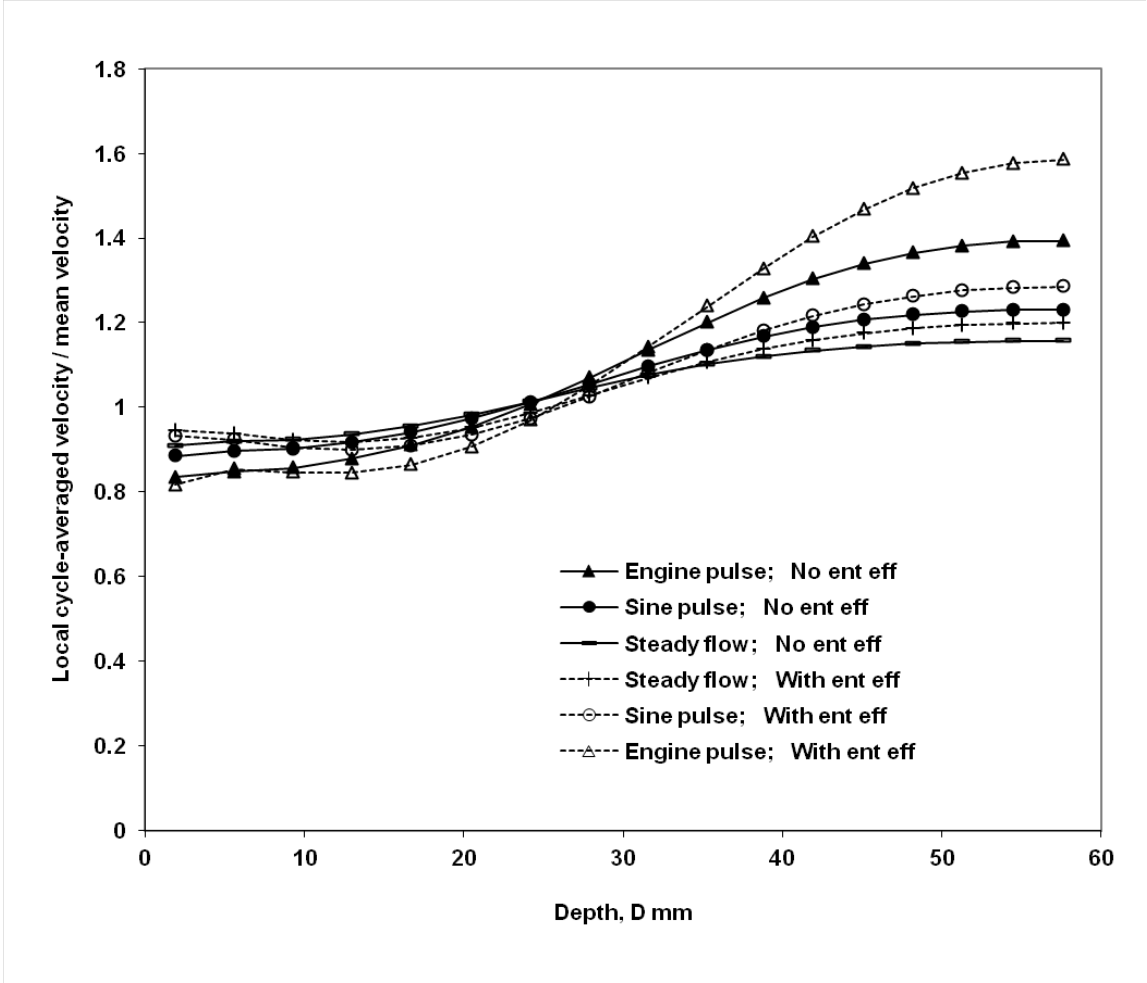
Local cycle-averaged velocity / mean velocity
Depth, D mm
Engine pulse; No ent eff
Sine pulse; No ent eff
Steady flow; No ent eff
Steady flow; With ent eff
Sine pulse; With ent eff
Engine pulse; With ent eff
0
0.2
0.4
0.6
0.8
1
1.2
1.4
1.6
1.8
0
10
20
30
40
50
60

Figure 2

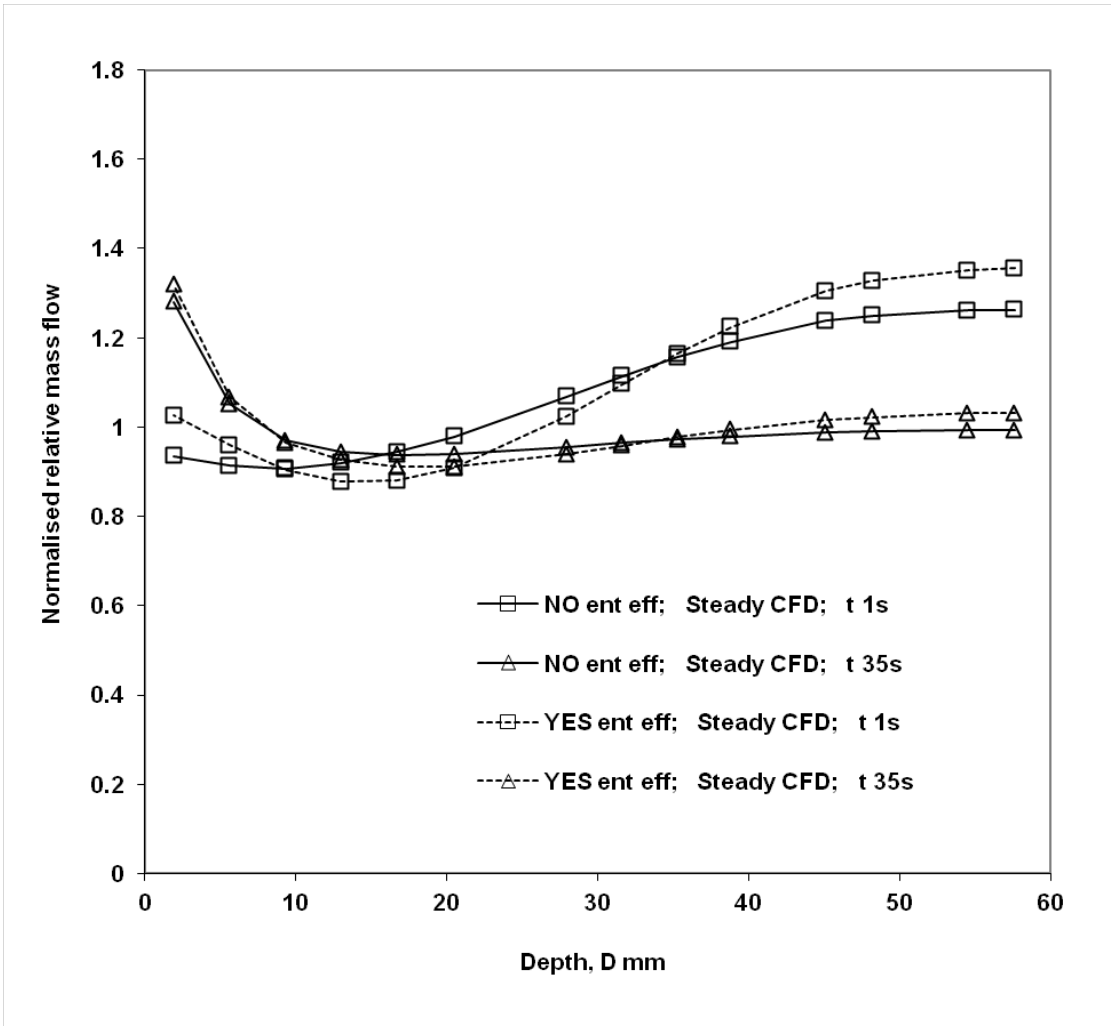
Normalised relative mass flow
Depth, D mm
NO ent eff; Steady CFD; t 1s
NO ent eff; Steady CFD; t 35s
YES ent eff; Steady CFD; t 1s
YES ent eff; Steady CFD; t 35s
0
0.2
0.4
0.6
0.8
1
1.2
1.4
1.6
1.8
0
10
20
30
40
50
60

Figure 3

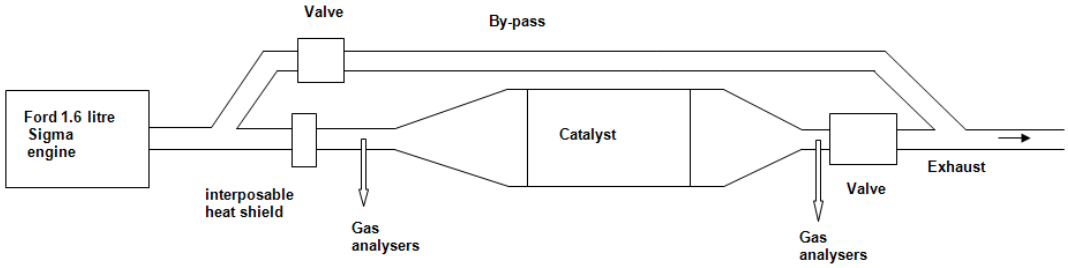
Valve
By-pass
Ford 1.6 litre
Sigma
engine
Catalyst
Exhaust
Valve
interposable
heat shield
Gas
analysers
Gas
analysers

Figure 4

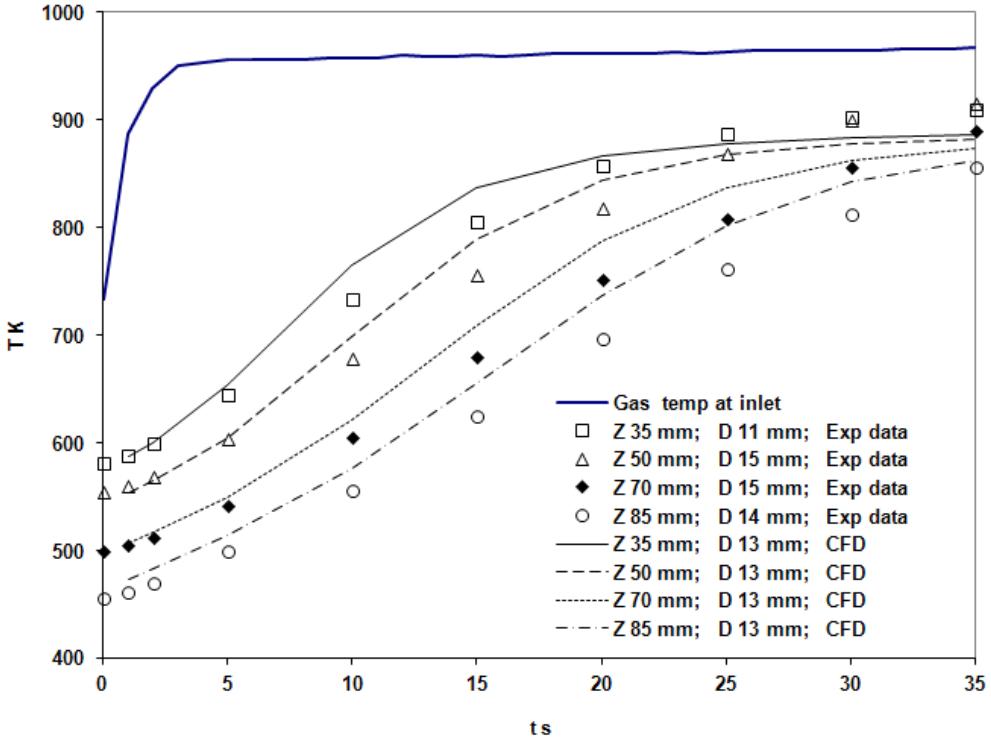
1000
900
800
700
600
500
400
T K
0
5
10
15
20
25
30
35
t s
Gas temp at inlet
Z 35 mm; D 11 mm; Exp data
Z 50 mm; D 15 mm; Exp data
Z 70 mm; D 15 mm; Exp data
Z 85 mm; D 14 mm; Exp data
Z 35 mm; D 13 mm; CFD
Z 50 mm; D 13 mm; CFD
Z 70 mm; D 13 mm; CFD
Z 85 mm; D 13 mm; CFD

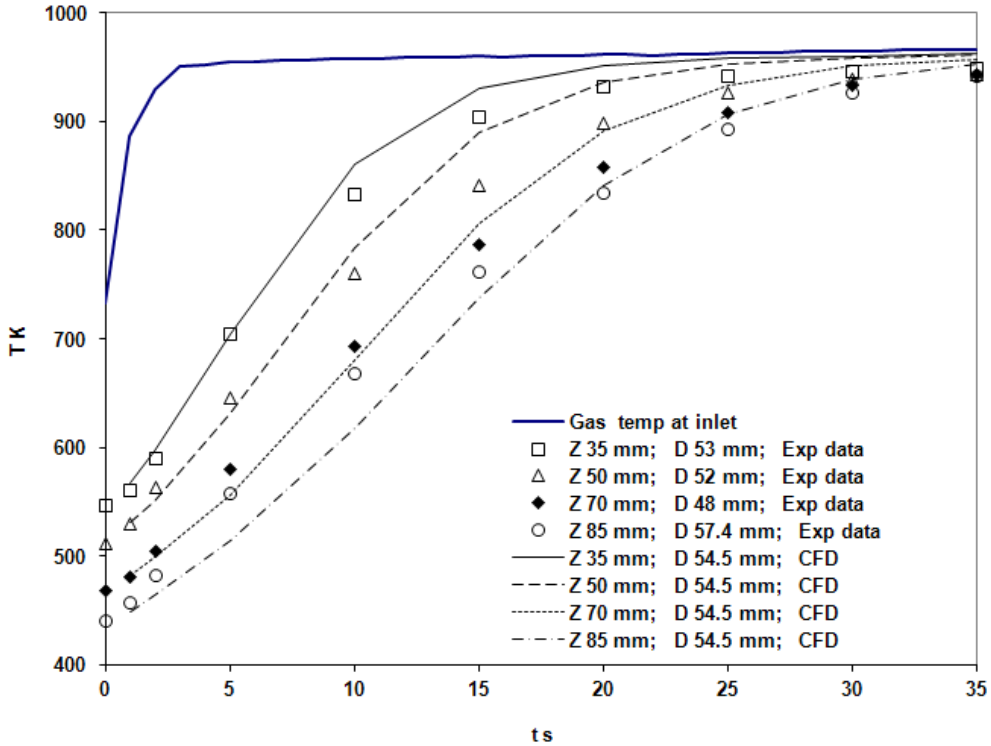
1000
900
800
700
600
500
400
T K
0
5
10
15
20
25
30
35
t s
Gas temp at inlet
Z 35 mm; D 53 mm; Exp data
Z 50 mm; D 52 mm; Exp data
Z 70 mm; D 48 mm; Exp data
Z 85 mm; D 57.4 mm; Exp data
Z 35 mm; D 54.5 mm; CFD
Z 50 mm; D 54.5 mm; CFD
Z 70 mm; D 54.5 mm; CFD
Z 85 mm; D 54.5 mm; CFD

Figure 5

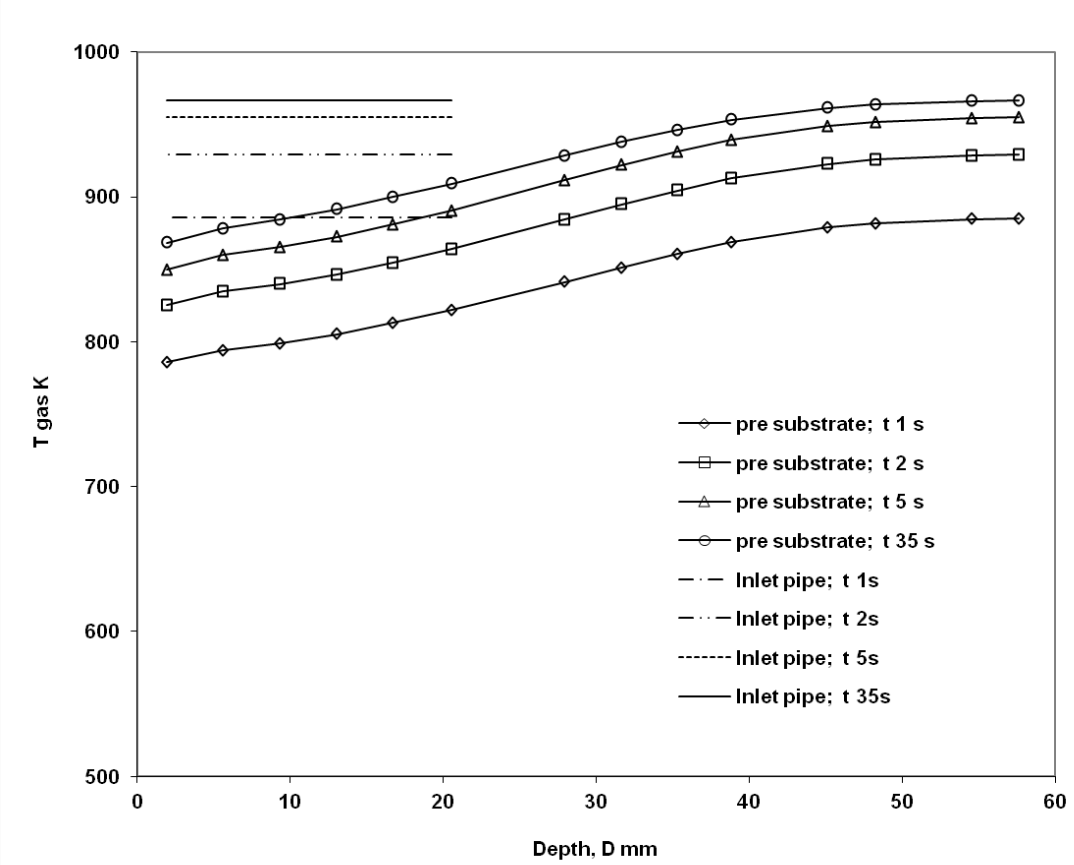
1000
900
800
700
600
500
T gas K
0
10
20
30
40
50
60
Depth, D mm
pre substrate; t 1 s
pre substrate; t 2 s
pre substrate; t 5 s
pre substrate; t 35 s
Inlet pipe; t 1s
Inlet pipe; t 2s
Inlet pipe; t 5s
Inlet pipe; t 35s

Figure 6

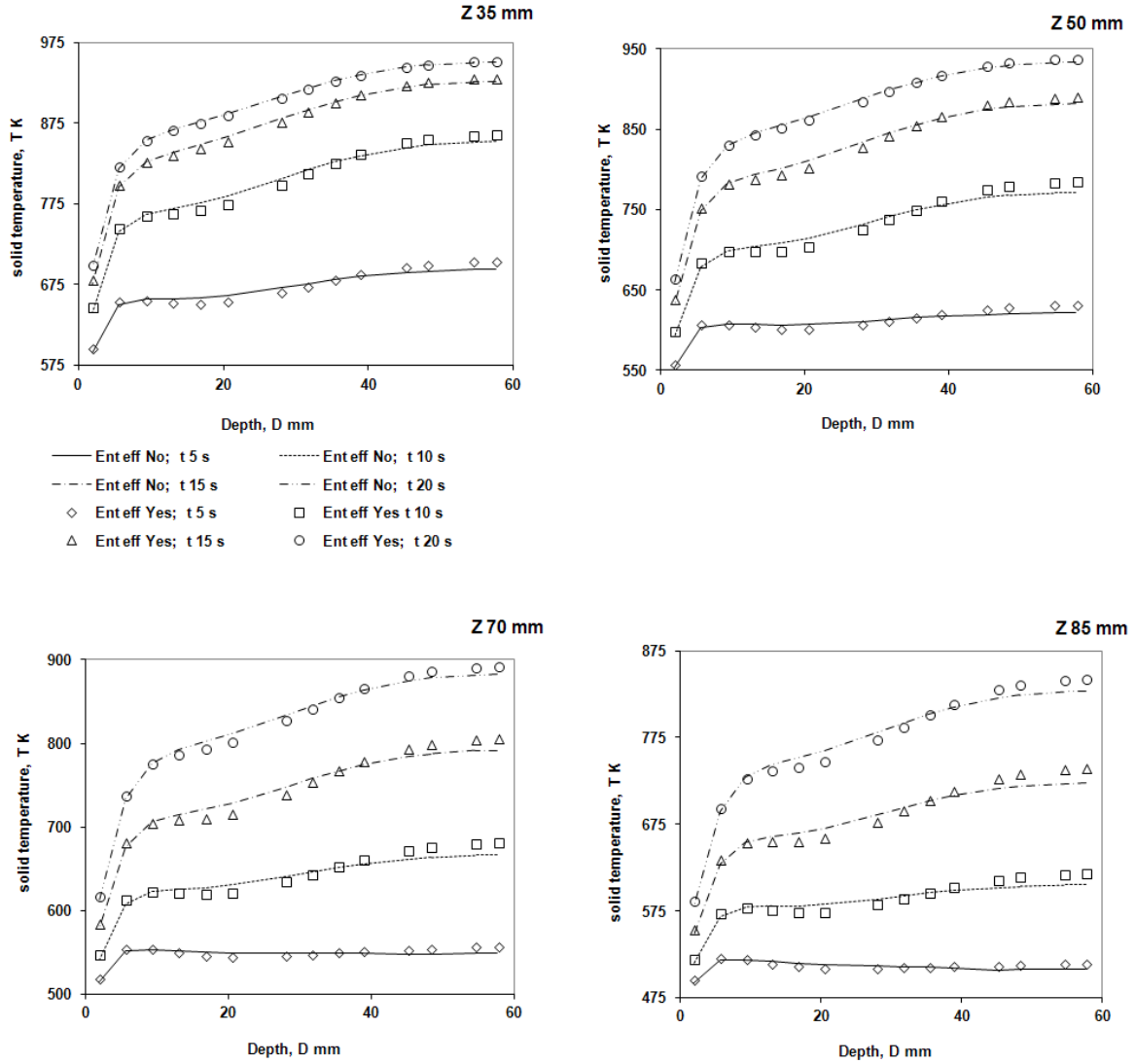
Z 35 mm
Z 50 mm
Z 70 mm
Z 85 mm
solid temperature, T K
Depth, D mm
Ent eff No; t 5 s
Ent eff No; t 10 s
Ent eff No; t 15 s
Ent eff No; t 20 s
Ent eff Yes; t 5 s
Ent eff Yes t 10 s
Ent eff Yes; t 15 s
Ent eff Yes; t 20 s

Figure 7

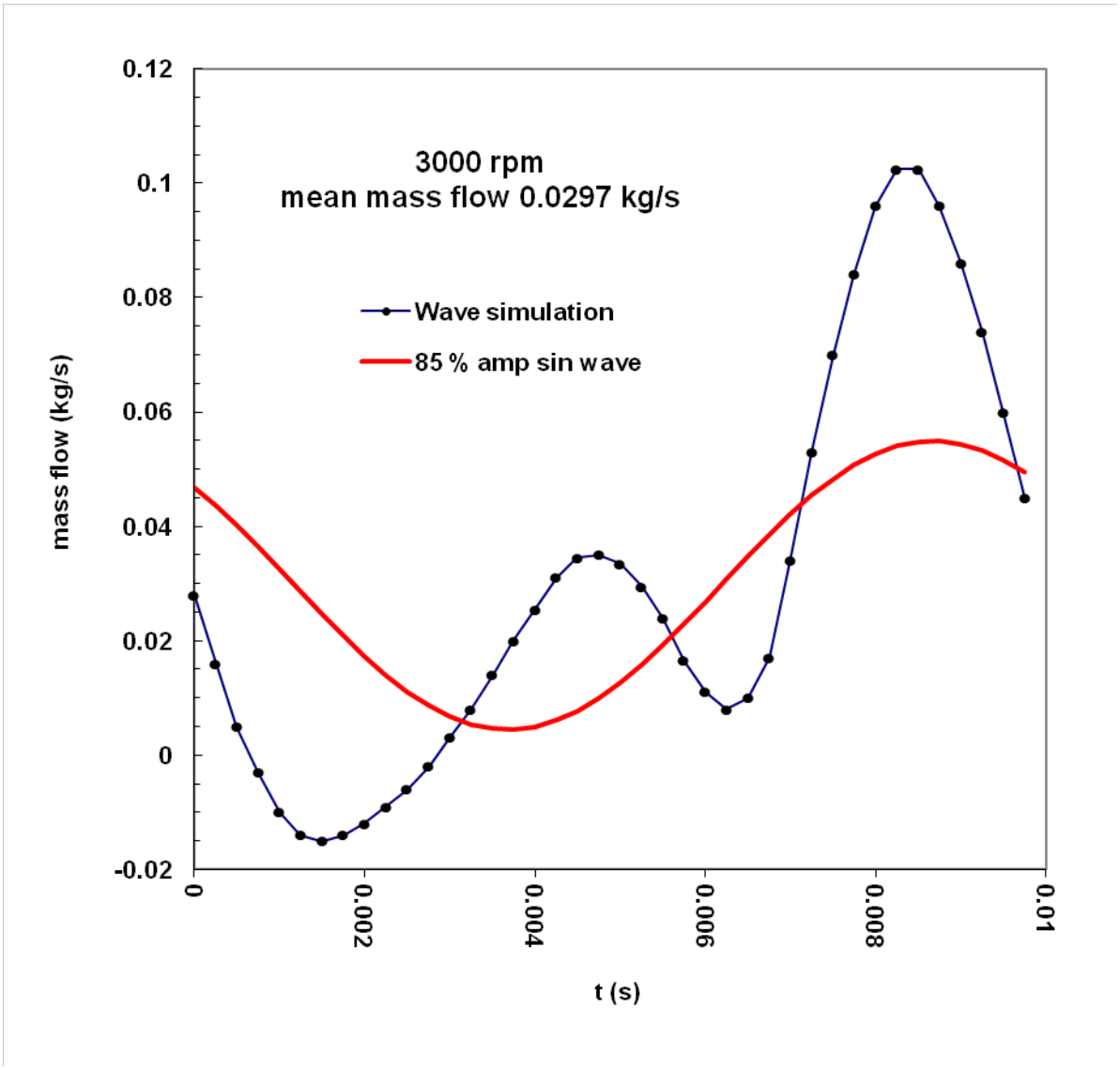
3000 rpm
mean mass flow 0.0297 kg/s
Wave simulation
85 % amp sin wave
mass flow (kg/s)
0.12
0.1
0.08
0.06
0.04
0.02
0
-0.02
0
0.002
0.004
0.006
0.008
0.01
t (s)

Figure 8

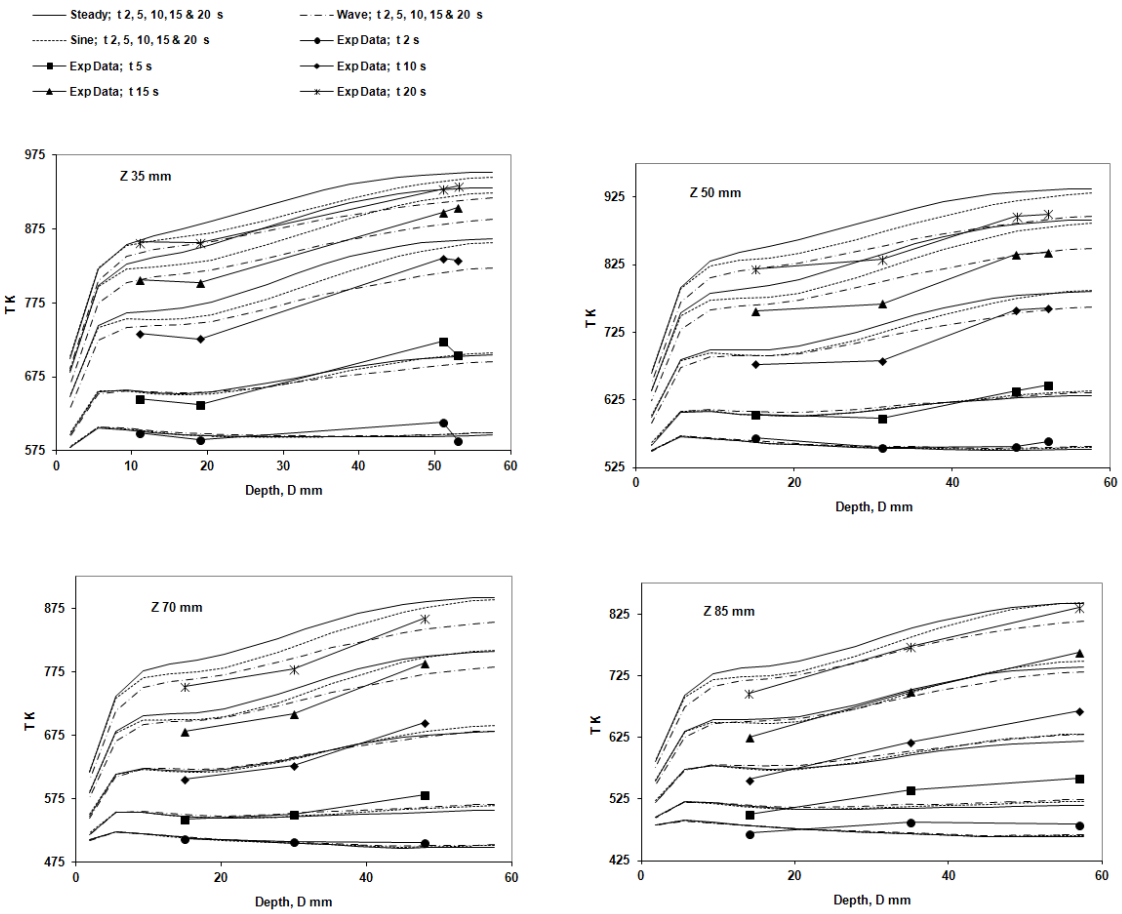
Steady; t 2, 5, 10, 15 & 20 s
Wave; t 2, 5, 10, 15 & 20 s
Sine; t 2, 5, 10, 15 & 20 s
Exp Data; t 2 s
Exp Data; t 5 s
Exp Data; t 10 s
Exp Data; t 15 s
Exp Data; t 20 s
Z 35 mm
Z 50 mm
Z 70 mm
Z 85 mm
T K
Depth, D mm

Figure 9

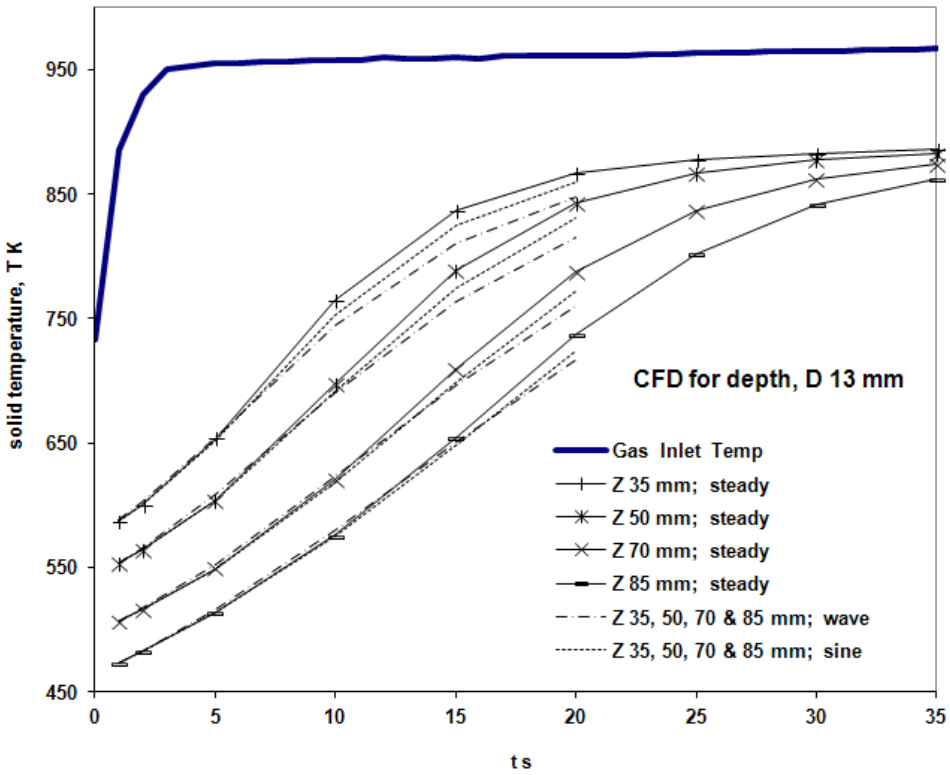
solid temperature, T K
950
850
750
650
550
450
0
5
10
15
20
25
30
35
t s
CFD for depth, D 13 mm
Gas Inlet Temp
Z 35 mm; steady
Z 50 mm; steady
Z 70 mm; steady
Z 85 mm; steady
Z 35, 50, 70 & 85 mm; wave
Z 35, 50, 70 & 85 mm; sine

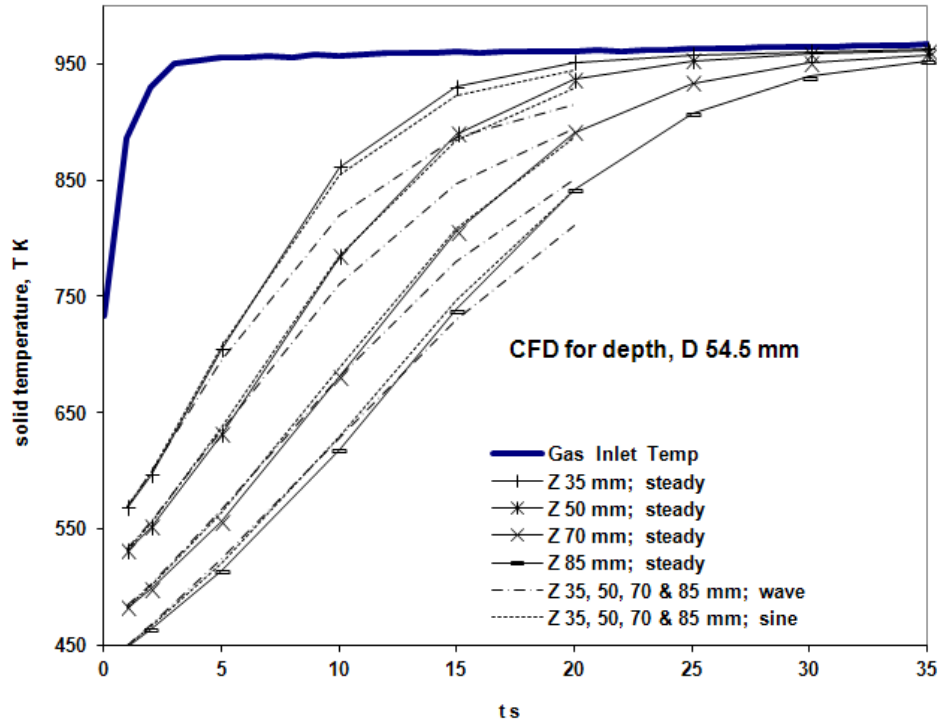
solid temperature, T K
950
850
750
650
550
450
0
5
10
15
20
25
30
35
t s
CFD for depth, D 54.5 mm
Gas Inlet Temp
Z 35 mm; steady
Z 50 mm; steady
Z 70 mm; steady
Z 85 mm; steady
Z 35, 50, 70 & 85 mm; wave
Z 35, 50, 70 & 85 mm; sine

Figure 10

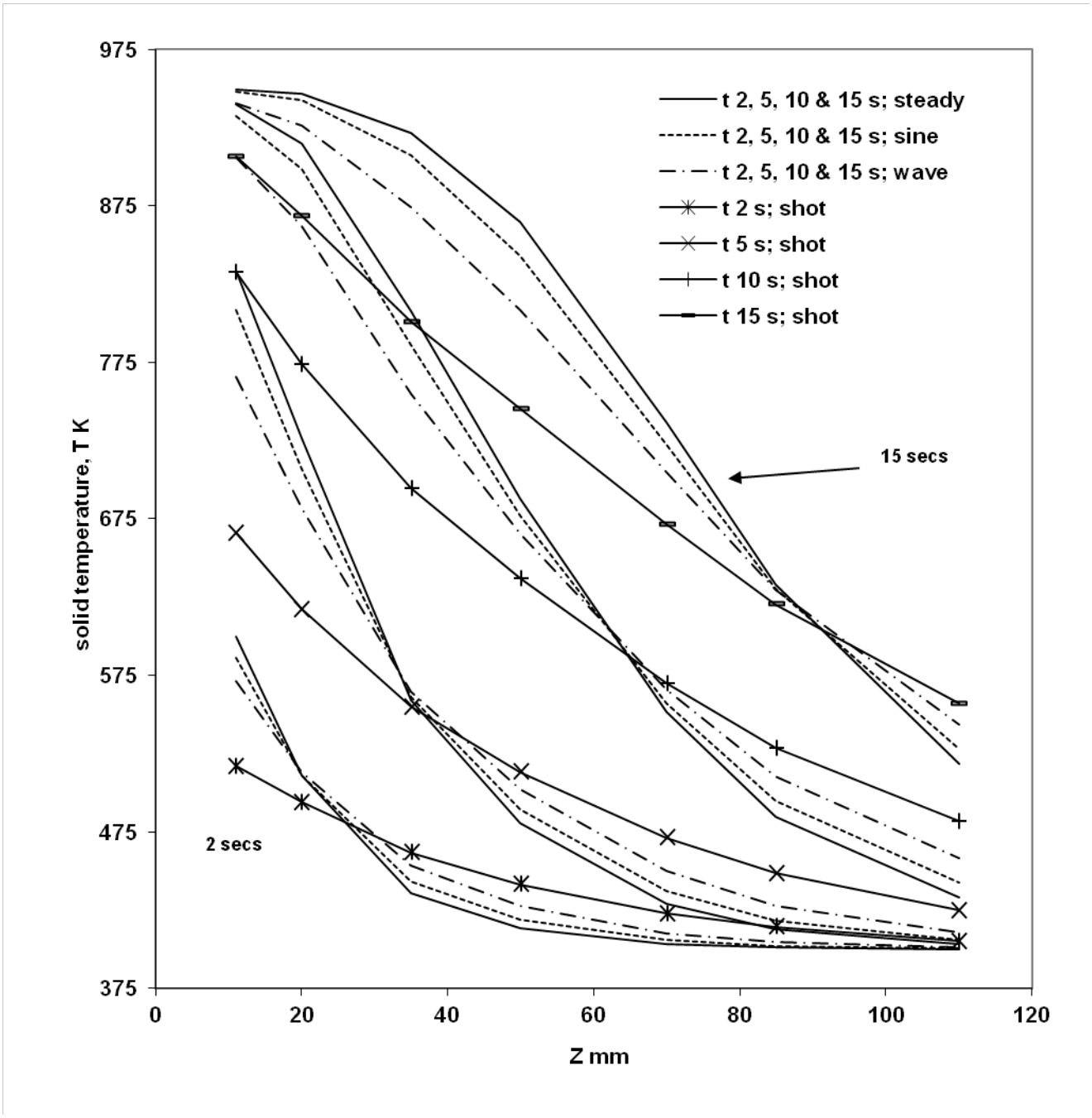
975
875
775
675
575
475
375
0
20
40
60
80
100
120
solid temperature, T K
Z mm
t 2, 5, 10 & 15 s; steady
t 2, 5, 10 & 15 s; sine
t 2, 5, 10 & 15 s; wave
t 2 s; shot
t 5 s; shot
t 10 s; shot
t 15 s; shot
15 secs
2 secs

Figure 11

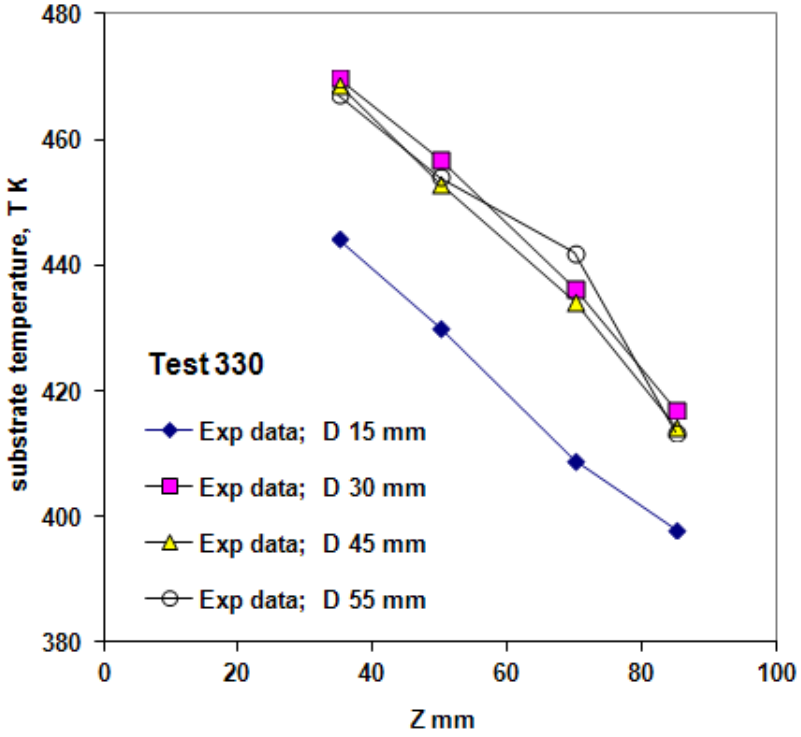
substrate temperature, T K
480
460
440
420
400
380
0
20
40
60
80
100
Z mm
Test 330
Exp data; D 15 mm
Exp data; D 30 mm
Exp data; D 45 mm
Exp data; D 55 mm

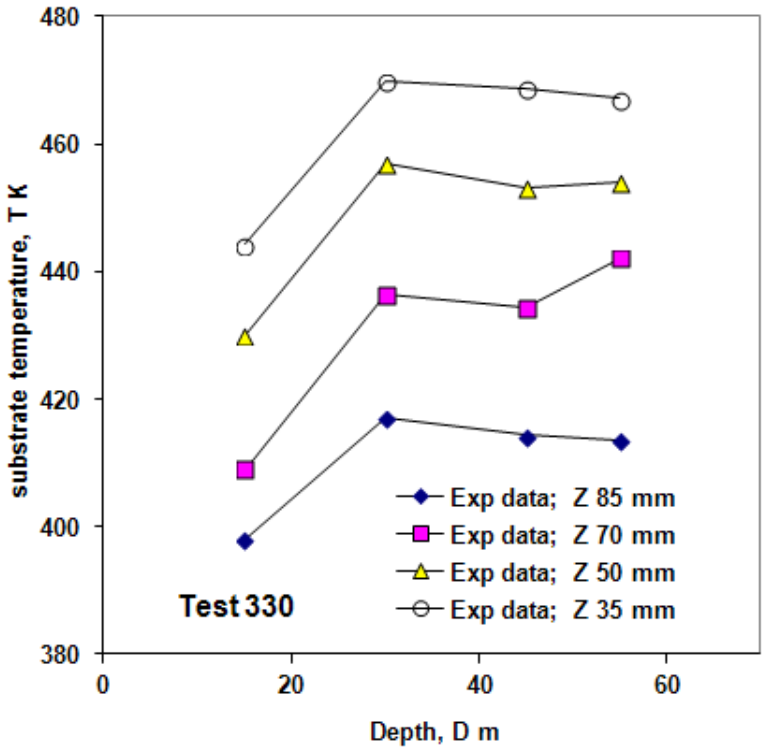
substrate temperature, T K
480
460
440
420
400
380
0
20
40
60
Depth, D m
Test 330
Exp data; Z 85 mm
Exp data; Z 70 mm
Exp data; Z 50 mm
Exp data; Z 35 mm

Figure 12

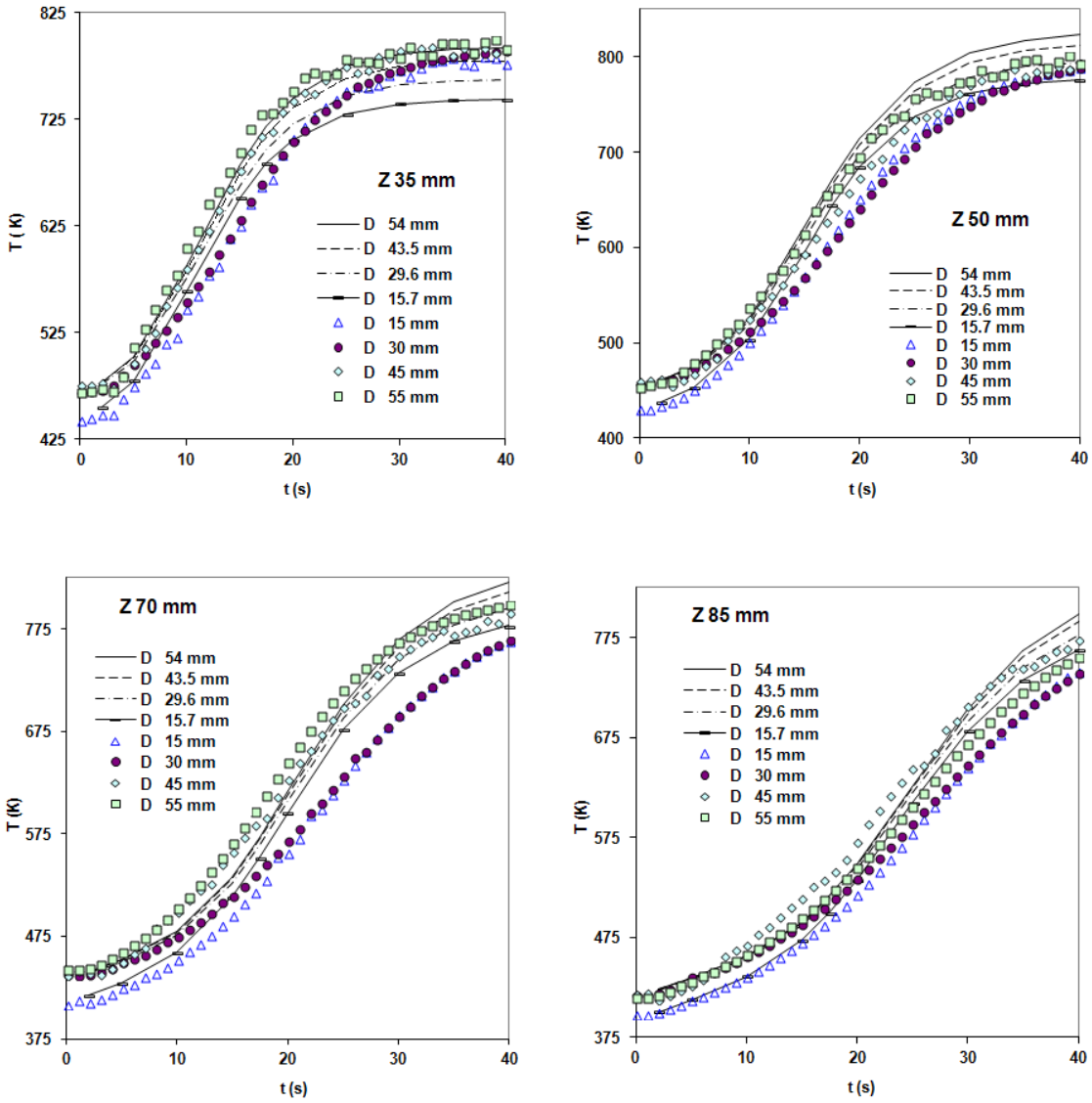
Z 35 mm
D 54 mm
D 43.5 mm
D 29.6 mm
D 15.7 mm
D 15 mm
D 30 mm
D 45 mm
D 55 mm
T (K)
t (s)
Z 50 mm
T (K)
Z 70 mm
Z 85 mm

Figure 13

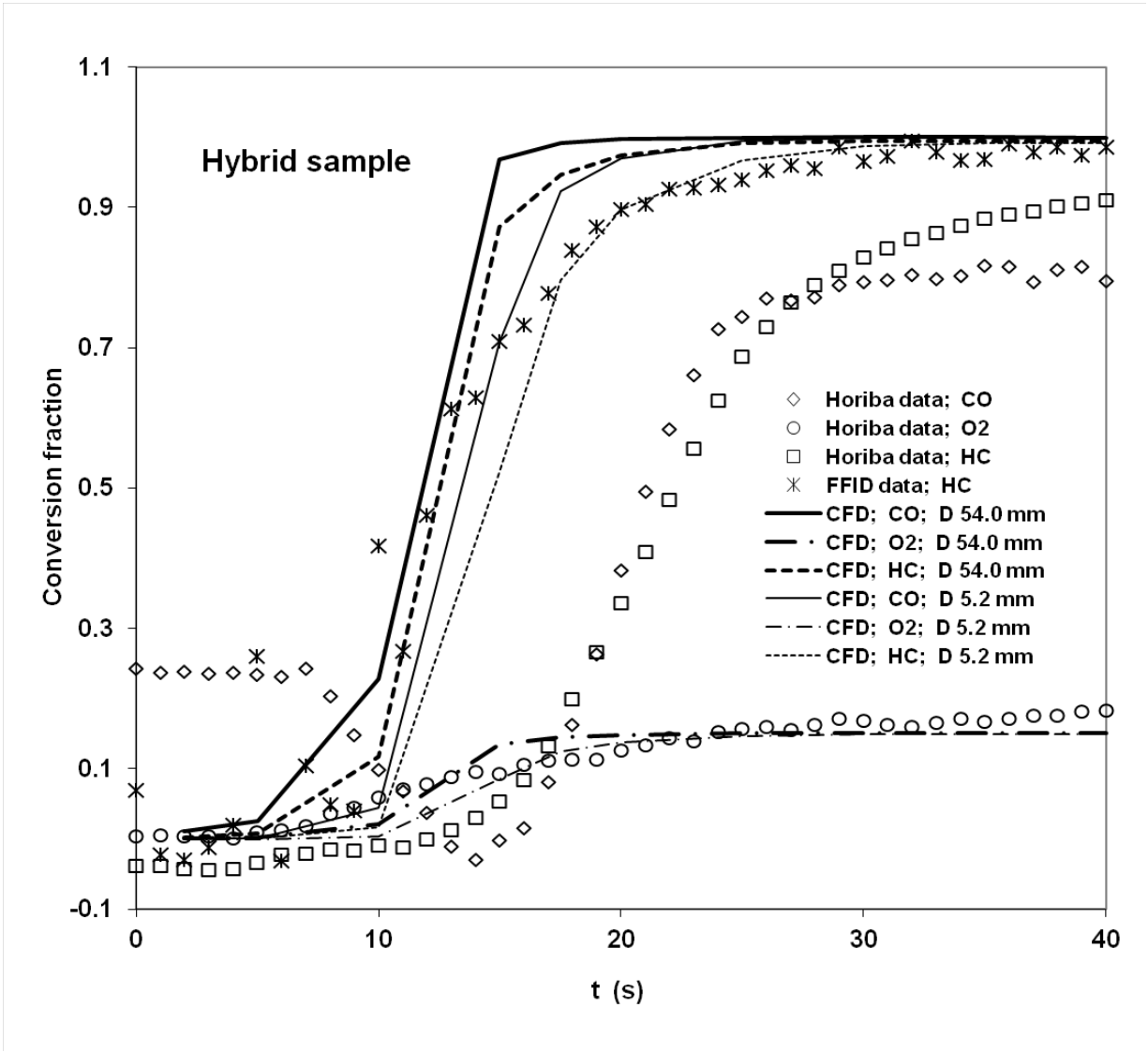
Hybrid sample
Conversion fraction
t (s)
1.1
0.9
0.7
0.5
0.3
0.1
-0.1
0
10
20
30
40
Horiba data; CO
Horiba data; O2
Horiba data; HC
FFID data; HC
CFD; CO; D 54.0 mm
CFD; O2; D 54.0 mm
CFD; HC; D 54.0 mm
CFD; CO; D 5.2 mm
CFD; O2; D 5.2 mm
CFD; HC; D 5.2 mm

Figure 14

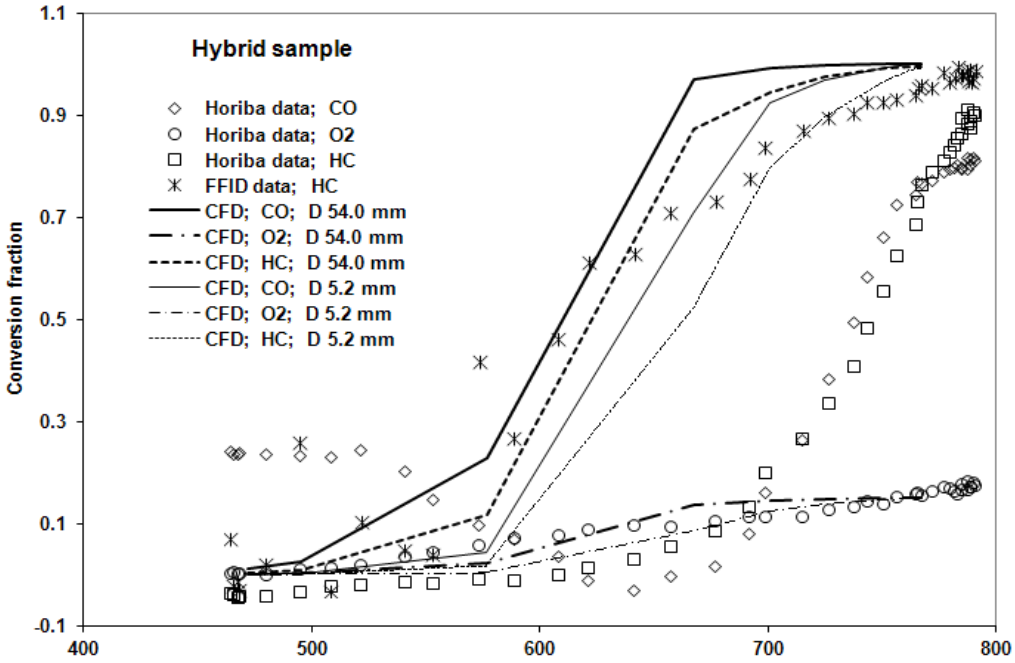

[A] Average temp. (K) at Z 35 mm between depth, D 15 mm and axis

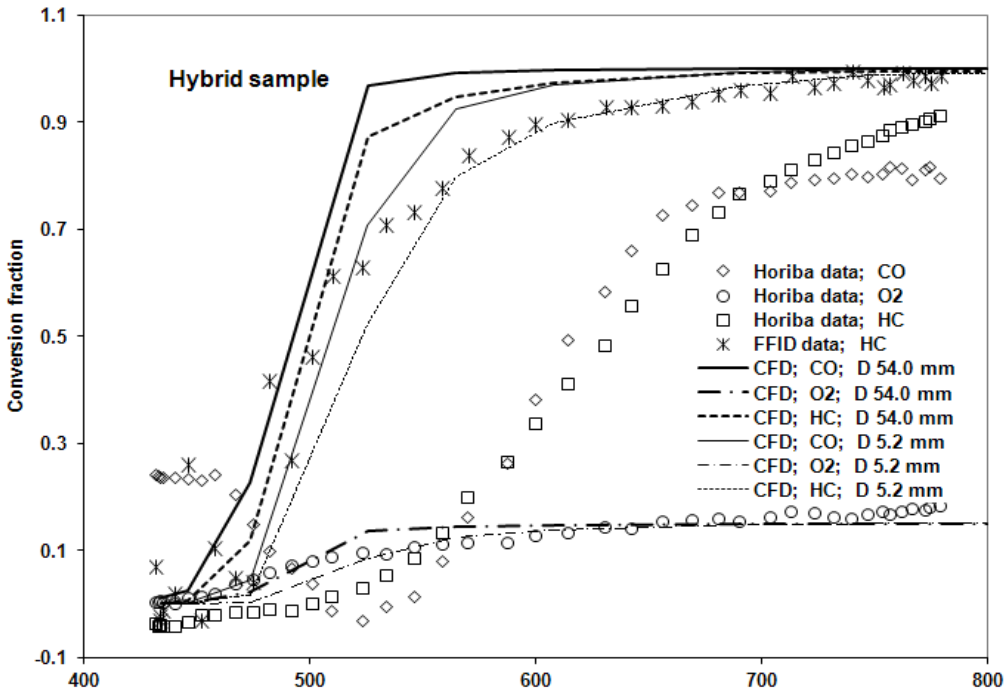

[B] Average temp. (K) at Z 70 mm between depth, D 15 mm and axis

Figure 15

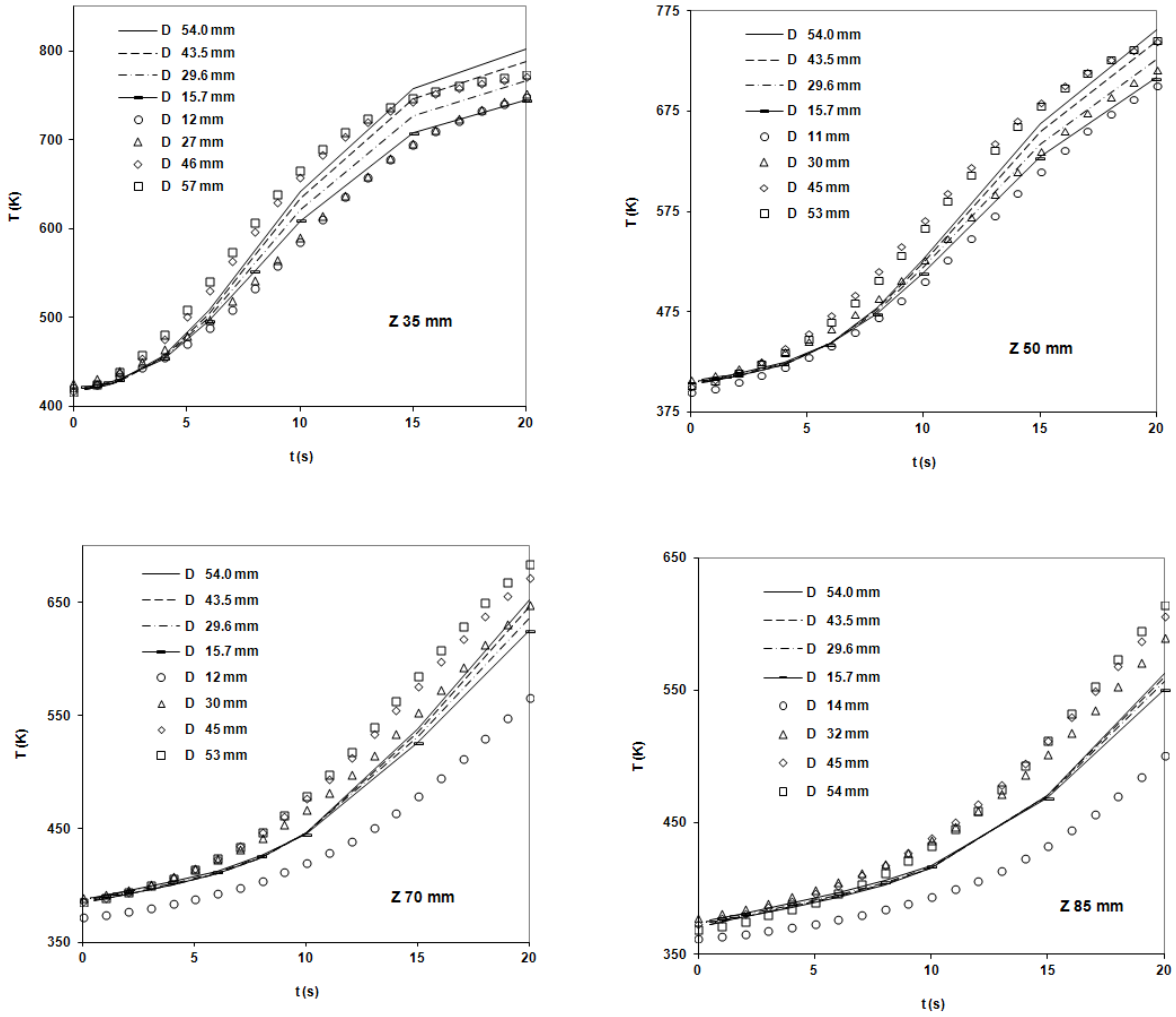
D 54.0 mm
D 43.5 mm
D 29.6 mm
D 15.7 mm
D 12 mm
D 27 mm
D 46 mm
D 57 mm
Z 35 mm
T (K)
t (s)
D 54.0 mm
D 43.5 mm
D 29.6 mm
D 15.7 mm
D 11 mm
D 30 mm
D 45 mm
D 53 mm
Z 50 mm
T (K)
t (s)
D 54.0 mm
D 43.5 mm
D 29.6 mm
D 15.7 mm
D 12 mm
D 30 mm
D 45 mm
D 53 mm
Z 70 mm
T (K)
t (s)
D 54.0 mm
D 43.5 mm
D 29.6 mm
D 15.7 mm
D 14 mm
D 32 mm
D 45 mm
D 54 mm
Z 85 mm
T (K)
t (s)

Figure 16

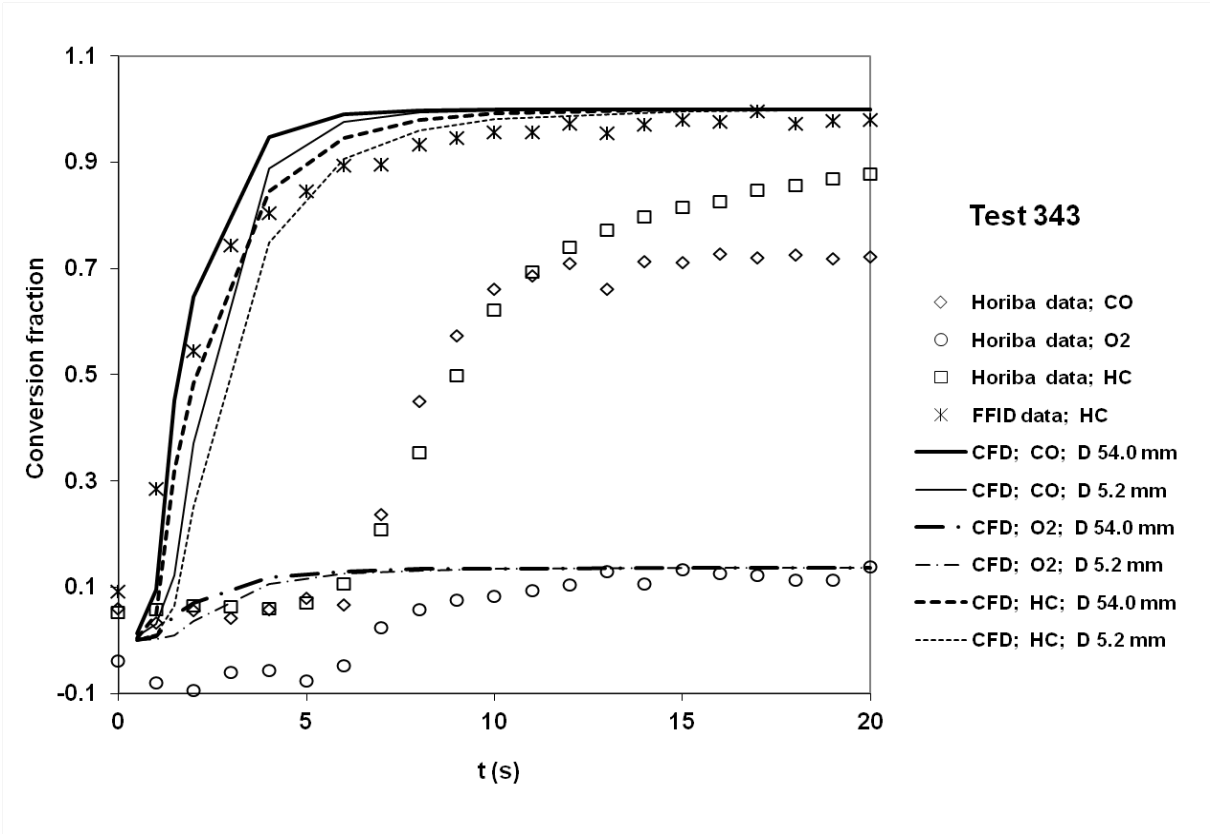
Test 343
Conversion fraction
t (s)
1.1
0.9
0.7
0.5
0.3
0.1
-0.1
0
5
10
15
20
Horiba data; CO
Horiba data; O2
Horiba data; HC
FFID data; HC
CFD; CO; D 54.0 mm
CFD; CO; D 5.2 mm
CFD; O2; D 54.0 mm
CFD; O2; D 5.2 mm
CFD; HC; D 54.0 mm
CFD; HC; D 5.2 mm

Figure 17

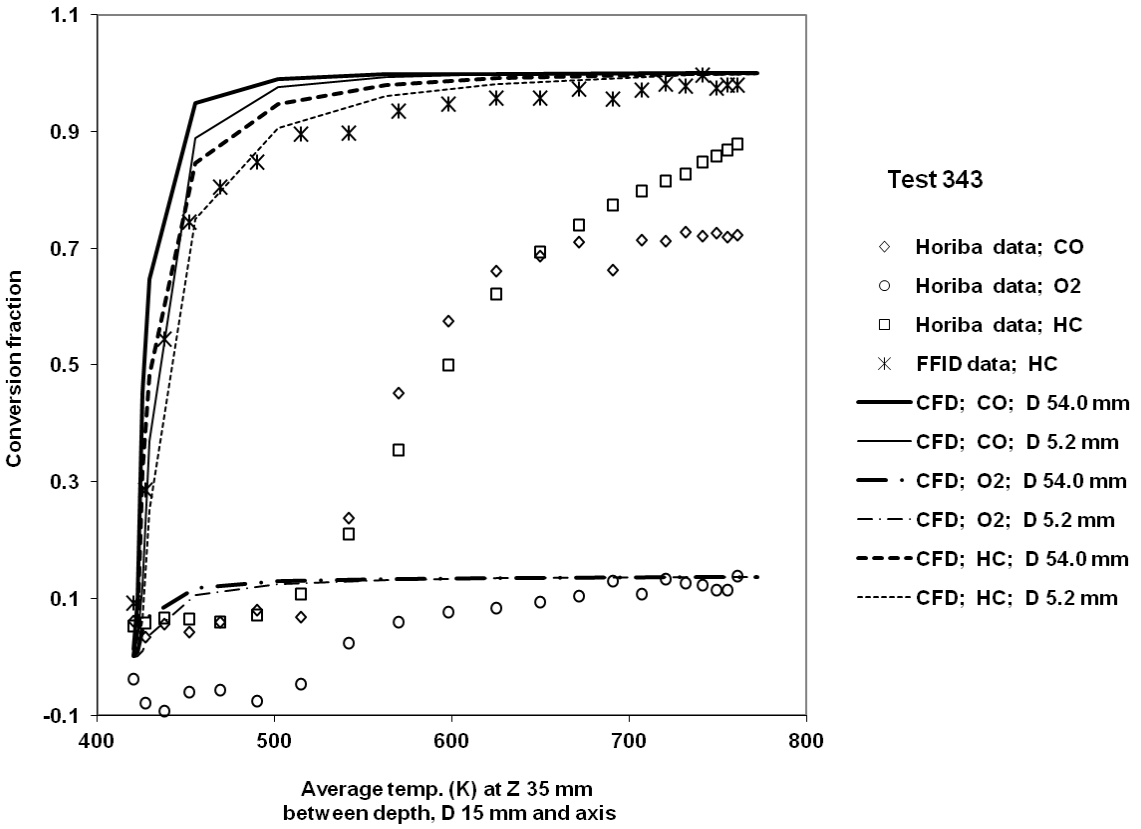
1.1
0.9
0.7
0.5
0.3
0.1
-0.1
Conversion fraction
400
500
600
700
800
Average temp. (K) at Z 35 mm
between depth, D 15 mm and axis
Test 343
Horiba data; CO
Horiba data; O2
Horiba data; HC
FFID data; HC
CFD; CO; D 54.0 mm
CFD; CO; D 5.2 mm
CFD; O2; D 54.0 mm
CFD; O2; D 5.2 mm
CFD; HC; D 54.0 mm
CFD; HC; D 5.2 mm

Figure 18